



Universität für Bodenkultur Wien
University of Natural Resources
and Life Sciences, Vienna

Master Thesis

Frequency Dependence of Mechanical Properties of Biological Materials

Submitted by

Lukas KRISMER, BSc

in the framework of the Master programme
Kulturtechnik und Wasserwirtschaft

in partial fulfilment of the requirements for the academic degree

Diplom-Ingenieur

Vienna, November 2021

Supervisors:

Univ.Prof. Dr. Jose Luis Toca-Herrera

Dr. nat. tech. Andreas Weber

Institute of Biophysics

Department of Nanobiotechnology

Affidavit

I hereby declare that I have authored this master thesis independently, and that I have not used any assistance other than that which is permitted. The work contained herein is my own except where explicitly stated otherwise. All ideas taken in wording or in basic content from unpublished sources or from published literature are duly identified and cited, and the precise references included.

I further declare that this master thesis has not been submitted, in whole or in part, in the same or a similar form, to any other educational institution as part of the requirements for an academic degree.

I hereby confirm that I am familiar with the standards of Scientific Integrity and with the guidelines of Good Scientific Practice, and that this work fully complies with these standards and guidelines.

City, date

Lukas KRISMER

24.11.2021



CONTENTS

Abstract	1
Kurzfassung	2
List of Abbreviations and Symbols	3
1. Motivation	5
2. Introduction	6
2.1. Biological materials	7
2.1.1. Hydrogels	7
2.1.2. Bacteria and Mechanics	8
2.1.3. Eukaryotic Cells and Mechanics	9
2.2. Mechanics	10
2.2.1. Time	10
2.2.2. Definitions	10
2.2.3. Material Models	14
2.3. Atomic Force Microscopy in Biomechanics	17
3. Materials and Methods	19
3.1. Agarose gel preparation	19
3.2. Cell culture & Sample Preparation	19
3.2.1. Cell culture routine	19
3.2.2. Sample preparation for AFM measurements	20
3.3. Bacterial culture & sample preparation	20
3.3.1. Bacterial culture	20
3.3.2. Sample preparation	21
3.4. Cantilever Preparation	21
3.4.1. Particle Glueing	22
3.5. Atomic Force Microscopy	23
3.5.1. AFM calibration	23

3.5.2.	Force Spectroscopy	24
3.5.3.	Data Analysis	27
4.	Results and Discussion	31
4.1.	Agarose Gels	31
4.1.1.	Force Distance Curves	31
4.1.2.	Comparison of the Agarose Gel concentrations for f-d curves	38
4.1.3.	Fittings Of the Force-Distance ^{3/2} Curves for Gels	40
4.1.4.	Youngs Modulus	45
4.2.	Bacterial Mechanics	47
4.2.1.	Force-Distance Curves	47
4.2.2.	Fittings Of the Force-Distance ^{3/2} Curves for Bacteria	48
4.2.3.	Youngs Modulus of E. coli	51
4.3.	MCF-7 Cell Mechanics	53
4.3.1.	Force Distance curves	53
4.3.2.	Fittings Of the Force-Distance ^{3/2} Curves for MCF-7	54
4.3.3.	Young's Modulus of MCF-7	59
4.4.	Power Law Rheology	60
5.	Conclusions	62
6.	References	64
7.	List of Figures	68
8.	List of Tables	71
9.	Acknowledgements	72

ABSTRACT

Adaption is a key task for every living species, especially for some of the smallest living entities. Cells and bacteria endure a wide range of external and internal stresses. Cells became so mechanically adapted on their environment, that they incorporate their stiffness accordingly. This allows blood cells to rush through the veins but enables cancer cells to metastasis. In this work time and stress dependent mechanical behaviour of three different biological specimen is inspected, MCF-7 cells, E coli. and Agarose gels, using an Atomic Force Microscope. A precise loading-rate was inflicted on the specimen at varying velocities. The elastic theory was applied on the data and power law fittings were performed. Here I show that cells have elastic moduli in the range of a few hundred Pa and that this modulus is strongly dependent on the frequency of the measurement. For bacteria, in this case gram-negative E. coli, a modulus of around 1 MPa was calculated, which also depends on the frequency of the measurement, but with a weaker power law exponent. Finally, two different agarose gels were investigated, and I show that there mechanical properties do not depend on the frequency of the measurement.

KURZFASSUNG

Anpassung ist ein Überlebensmerkmal für jede lebende Spezies, insbesondere für die kleinsten lebenden Teilchen. Zellen und Bakterien müssen eine Vielzahl von äußeren und inneren Belastungen ertragen. Zellen passen sich mechanisch derart an ihre Umgebung an, dass deren Steifigkeit von der Umwelt gravierend beeinflusst wird. Dies ermöglicht es den Blutzellen schadlos durch die Venen zu fließen. Andererseits ermöglicht ein weicherer Phänotyp es Krebszellen zu metastasieren. In dieser Arbeit wird das zeit- und stressabhängige Verhalten an drei verschiedenen biologischen Proben - MCF-7-Zellen, E. coli, und Agarosegelen - unter Verwendung eines Rasterkraftmikroskops untersucht. Die Proben wurden bei unterschiedlichen Geschwindigkeiten einer genau definierten Belastung ausgesetzt. Die Ergebnisse wurden mittels elastischer Theorie und einem Potenzgesetz ausgewertet und interpretiert. Während Zellen sehr weich sind mit einem Elastizitätsmodul im Bereich von einigen hundert Pa, sind E. coli um ein Vielfaches steifer (im Bereich von MPa). Die Agarosegele verhalten sich elastisch, während die Daten von Bakterien und Zellen einem schwachen Potenzgesetz folgen.

LIST OF ABBREVIATIONS AND SYMBOLS

AFM	Atomic Force Microscope
DMEM	Dulbecco's Modified Eagle Medium
DMSO	Dimethylsulfoxide
E	Young's Modulus, in Pascal
EtOH	Ethanol
F	Force, in Newton
k	Spring constant, in Newton/Meter
k_b	Constant of Boltzmann
LB	Lysogeny Broth Medium
MCF-7	Michigan Cancer Foundation, Cell Line
Pa	Pascal, Units of Pressure
PBS	Phosphate Buffer Saline
PEI	Polyethyleneimine
QI	Quantitative Imaging
R_c	Radius of indenter
rpm	Rounds per minute
SPM	Surface Probe Microscope
T	Temperature
UV/O	Ultraviolet-Ozone cleaning
α	Power law exponent
δ	Deformation, in meter
ν	Poisson ratio
ω	Frequency
ε	Strain
σ	Stress
τ	Relaxation time, shear stress
η	Viscosity
ΔL	Change in Length
A	Area of contact
G	Shear Modulus, in Pa
G'	Storage Modulus
G''	Loss Modulus
Z_p	Position of piezo in z-direction
δ_c	Deformation of cantilever
δ_s	Deformation of Sample

N Number of measurements/experiments

1. MOTIVATION

Forces shape the environment on a macro- and microscale. For many biological materials the environment defines the shape, size, and stiffness of the living beings. Over the years scientists discovered that small biological structures, such as cells, or bacteria are not solely controlled by chemical stimuli, they react on mechanical stress as well.

From a mechanical point of view, a popular model is to compare cells with gels. Since the human body is nothing more than a well-structured accumulation of specialized cells and a kind of mechanical and thermal machine, we contain different gels with varying viscoelastic properties beneath the skin. Cells react on this microenvironment and adopt their mechanics accordingly. Cancer cells become softer prior to metastasis. Not just cells allow humans to live. We live in symbiosis with billions of bacteria. *Escherichia coli* is one of them and vital for our digestive system. At the same time *E. coli* causes many deaths by inflicting dehydrating sicknesses.

The main motivation of this work is giving an overview of the mechanical models applied on biological matter, to compare the mechanical properties of cells, bacteria and their microenvironment, which is modelled by a simple hydrogel.

2. INTRODUCTION

Living beings interact with their surroundings in many different ways and the study of how mechanical interactions take place between different biological materials is intriguing. The ability of a whole organism to move and survive depends on tightly organized chemical and mechanical processes at the tiny scales of proteins and cells, going up to tissue and whole organism scale [1]–[5]. Therefore, the field of mechanical properties of biological materials at different scales, from nm to m, has progressed immensely in the last decades, aiming to understand the role of mechanical forces in biology [6].

There are many different examples of why mechanical forces are important in biology. Living organisms must be able to detect, sustain and also interact the different physical forces that the environment embeds on them. A simple example is the gravitational force that we are all under, and only through the interplay of the skeleton with soft muscle and tendon tissue are we able to move around. This movement itself is empowered by reactions of molecular motors at the nanoscale, where ATP hydrolysis is used to change the conformation of motor proteins which in the end enables muscle fibre movement [7]. Similarly, basic body functions of the respiratory and circulatory system require mechanical driving forces that are generated by expansion/compression cycle of organs such as the lung and the heart [8], [9]. Again, these functions are based on molecular and cellular scale events. It is therefore no surprise that in different states of disease that change the mechanical properties of e.g. cardiomyocytes or their surrounding extracellular matrix, fatal heart disease can be a result [10]–[12]. Other examples of the importance of mechanical forces in biology include embryonal development, cellular migration (which is important e.g. in cancer formation), adhesion, and many more [13]–[17].

One important aspect of studying mechanics in biological materials is to properly investigate the mechanical properties of the materials at the different scales [18]–[20]. This can be quite a complicated task, as biological materials are small (ranging from nm for proteins, to μm for bacteria and dozens of μm for cells, and up to the cm range for hydrogels), soft and often “sticky”. In addition, as most of these materials are made by complex, hierarchical self-assembly processes, they tend to exhibit quite complex mechanical behaviour that is not easily modelled [6], [18], [21]–[32]. Therefore, this thesis sets out to study three very different biological materials (Agarose gels, bacteria, and breast cancer cells) using Atomic Force Microscopy. In the following section I will provide basic information about the different types of materials under study, introduce basic concepts of mechanics and will finally describe AFM as a method well-suited to study these complex materials.

2.1. BIOLOGICAL MATERIALS

There are many different definitions of biological materials. In this thesis I will follow the definition that these materials include all materials that are derived from living organisms or used for culturing these. The materials under study here include a simple hydrogel (Agarose), gram-negative bacteria and epithelial breast cancer cells.

2.1.1. HYDROGELS

A hydrogel is defined as a water-containing polymeric gel structure that is non-soluble in water. Hydrogels are produced by polymerization processes in liquid [33]–[37]. Monomers in hydrogels are cross-linked either chemically or physically. Different types of base materials can be used to produce hydrogels, include collagen, agar, acrylamide, gelatine, and more. The applications for hydrogels are manifold, but they are probably most often used as scaffolds for biomedical engineering purposes [38], [39]. One major feature of these materials is that their mechanical properties can be readily modified using different cross-linking or changing the polymer concentration [40], [41]. Hydrogels are used to mimic the mechanical and chemical properties of tissue. As an example, Agarose gels are used as substrate to grow cells or bacteria. This can be excelled by building up 3D instead of the 2D use as substrate. To inject cells in a 3D gel has the advantage to mimic its natural environment even better. Especially in the field of stem cell differentiation, hydrogels have been extensively used, because the gel stiffness can be used as differentiation signal. As an example, for mesenchymal stem cells the impact of the gel's stiffness defines the phenotype of the stem cell lineage [42], [43]. Stiffer gels lead to osteoplastic phenotype, while softer gels lead to a myospastic expression.

A hydrogel is a mixture of a crosslinked solvent and water – “hydro”. Hydrogels behave like a saturated sponge, where the sponge itself is the cross-linked gel matrix. When exerted to external force, water moves and desaturates the sponge locally. When the force decreases the liquid “flows” back into the sponge and it is as it was before. The cross-linked network behaves elastically. The water distribution within the gel exhibits a viscous behaviour. A mechanical model to describe gels is the poroelastic model [44], [45]. The movement of water within the gel is limited by the size of pores, so the water needs to diffuse through the cross-linked network. The concentration defines the number of cross-links. The more links, the stiffer the gel, the more force is needed to distribute the water within the gel. The stiffness of hydrogels can be tuned from low Pa to high MPa region, depending on the used monomer, cross-linking strategies and applied concentrations.

In this thesis I will use simple Agarose gels as an exemplary hydrogel and study them at the microscopic level using AFM. This will provide insights into the mechanical properties of the gels.

2.1.2. BACTERIA AND MECHANICS

Bacteria are small, μm -sized organisms that come in many shapes and have been found in nearly all habitats on earth [46]. Their major load-bearing structure of bacterial cells is thought to be the cell envelope [47]–[49]. They can be classified in two kinds: gram-negative and gram-positive. They are classified this way because of the gram-staining technique. The outer shell of gram-positive bacterial cells consists of a thick layer of peptidoglycan. The inner layer of its membrane is called plasma membrane. In between the plasma membrane and the Peptidoglycan layer lies a thin periplasmic space. Opposing to gram-positive bacteria, gram-negative bacteria do have an outer membrane and the plasma membrane on the inside. In between these membranes lies the periplasm with a thin layer of peptidoglycan. Peptidoglycan is a complex macromolecule that is made up of stiff glycan chains that are interconnected via flexible small peptide chains. As there is a large difference in concentration of molecules between the inside of bacterial cells and the outside, the bacterial envelope must withstand an enormous turgor pressure in the range of MPa, which is similar to the pressure inside a bicycle tire. In addition, the envelope is the major shape defining structure, which is intriguing as this means that there is mechanical anisotropy.

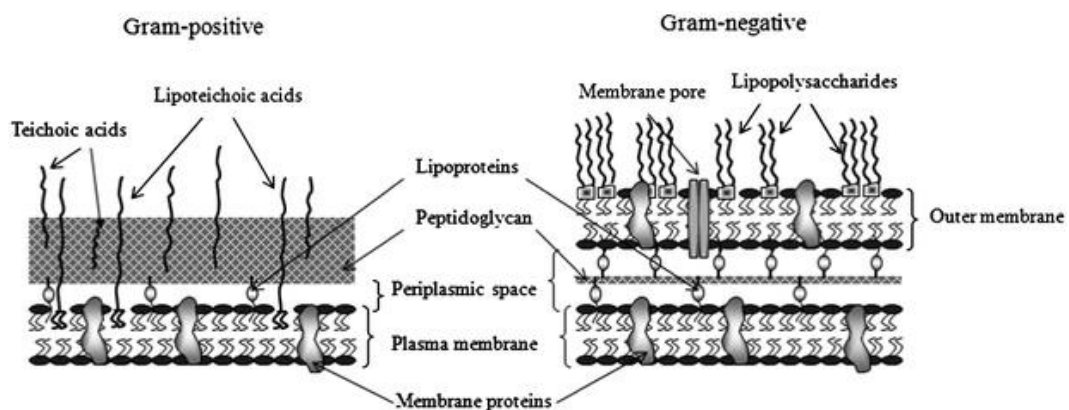


Figure 2-1. Architecture of the bacterial cell wall. Left part of the figure shows gram-positive and right part shows gram-negative cells. Figure taken from Vadillo et al, *Soft Matter*, 2011.

The study of bacterial mechanics goes back to the middle of the last century, and only in recent years the addition of AFM to the mechanical measurement toolkit has provided the ability to measure the properties at those small scales. Bacteria are found to be stiff biological materials, with Young's Modulus in the range of MPa [50]. Still, different creep and dynamic experiments have shown that bacteria show viscoelastic solid-like behaviours.

Investigating the mechanics of bacteria is interesting, as it will give insights in how the self-organization of the bacterial structures is able to withstand such large pressures. In addition, still today there is no consensus on how bacteria produce enough mechanical force to withstand the pressure differences in cell division. Therefore, studying bacterial mechanics is still a hot topic.

In this work I have investigated an *E. coli* strain that is normally used in fermentation processes. *Escherichia coli* are known for triggering many diseases, such as diarrhoea and vomiting. But they play a significant role within our digestive system as well. *E. coli* are gram negative.

2.1.3. EUKARYOTIC CELLS AND MECHANICS

A cell is a well-structured biological puzzle part. It can live by itself, but it can be puzzled together to build larger structures. Cells are the smallest living compartments and are organized in the tissue in multicellular structure, where each cell has its specialized function [7].

The cell consists of different compartments: The membrane envelopes the cytoplasmic compartment and serves as a separation from the outside, while incorporating many different transport proteins to ensure transport of nutrients inwards and efflux of cell waste and other molecules. Inside the cytoplasm, the cytoskeleton is residing. It is a complex meshwork of different filaments. There are three key filaments that build up a cell's skeleton [51]. The microtubule is the most rigid filament and it builds long hollow cylindrical tubes. The actin filaments have shorter persistence lengths than the microtubule when a single filament is compared. They are made up by polymerization of globular actin. Inside the cell, there are many different actin cross-linking proteins that are used by the cell to form different actin structures. These structures are needed e.g. to keep cell shape and mechanics, for migration and for adhesion purposes [52]. Close to the membrane lies a dense net of actin filaments, the actin cortex that is thought to be primarily responsible for the cell's stiffness [53]. The third group of filaments connects the previous, the intermediate filaments. Today there is still a debate ongoing in the field of the different roles of cytoskeleton and other cell elements in defining the mechanical properties of cells. Cells have been shown to behave as viscoelastic materials and many different modelling approaches have been applied to capture their behaviour.

Cells are very adaptable and have many different functions. One of the challenges a cell faces is to resist and respond to external stress. Vital human functions, such as breathing apply great mechanical stress on epithelial lung cells. Blood cells need to resist blood

pressure and visco-dynamic drag forces. Therefore, there must be an interplay of resistance to deformation, while at the same time being deformable enough to properly perform the needed functions.

One field where the investigation of the cell mechanical properties is especially relevant is in cancer [54], [55]. Cells have been shown to become softer over the course of cancer progression. In addition, the adhesive properties of cells appear changed during cancer. In this study, MCF-7 cells are used as a model for epithelial breast cancer to measure cellular mechanics.

2.2. MECHANICS

External mechanical forces are omnipresent. Gravitation keeps us ground-based, a cool summer breeze or the impact on the feet while walking around the corner exerts external forces on the body. Resisting, reacting and interacting these forces is one fundamental keystone that enables life. Newtons third law states: “*actio est reactio*”. This implies that for a body to maintain its shape, internal forces need to act equally in size but in opposite direction of the external forces. This accounts for all things such as molecules, fungi, tents, viruses, stones, cells, or humans.

Another reason for investigating mechanics on biological specimen is that it can trigger chemical responses that lead to the adoption of stress or triggering a chemical signal. This is called mechanobiology, and the signalling transduction of a mechanical signal to a biochemical one is called mechanotransduction.

2.2.1. TIME

Prior to the exploration of mechanical properties, it is advised to consider time as a relevant dimension. Is the mechanical property time dependent? If not, then time does not need to be considered. When it does play a role, the length of the time scale becomes relevant. A concept that takes this into account is the Deborah number.

$$De = \frac{\textit{relaxation time}}{\textit{measurement time}}. \quad \text{Eq. 1}$$

The Deborah number puts the material response in relation to the duration of an observation. When it is close to 0 then the body behaves like a liquid, when it is large the body exhibits a solid like behaviour.

2.2.2. DEFINITIONS

Prior to the material models are some basic definitions. Stress (σ) is Force (F) per Area (A). It is measured in Pascal (Pa).

$$\sigma = \frac{F}{A}. \quad \text{Eq. 2}$$

In normal stress a force acts normal on a surface of the body, whereas for shear stress (τ) the force acts in the plane of the surface. Stresses acting on a certain point are described in the entirety of stresses in that area.

$$S_{2D} = \begin{bmatrix} \sigma_x & \tau_{xy} \\ \tau_{yx} & \sigma_y \end{bmatrix}, \quad \text{Eq. 3}$$

Strain (ε) is the ratio of the actual length to the original length L_0 . It is dimensionless and the uniaxial strain is defined as

$$\varepsilon = \frac{\Delta L}{L_0}, \quad \text{Eq. 4}$$

where ΔL is the change in length.

2.2.2.1. ELASTICITY

The relationship of stress to strain in linear elasticity is called Young's Modulus (E) and is defined as

$$E = \frac{\sigma(\varepsilon)}{\varepsilon}. \quad \text{Eq. 5}$$

The Young's Modulus is a three-dimensional material property. It can be applied for reversible, elastic deformations. Stress that acts along one axis leads not just to a change in length in that direction, but to change of length in the normal direction as well. The Poisson number defines the ratio of transversal to axial strains. Usual values for μ are 0.2 - 0.5.

$$\mu = \frac{\Delta d}{d} : \frac{\Delta l}{l}, \quad \text{Eq. 6}$$

In the case of the materials studied here, the Poisson ratio is always thought to be 0.5, which means that the materials are incompressible. Shear forces (τ) act tangential to a surface where it acts. The "tilt" is defined through a shear angle (α). L is the distance of the two surfaces.

$$\tau = \frac{F}{l^2}, \quad \text{Eq. 7}$$

$$\tau = G * \alpha, \quad \text{Eq. 8}$$

G is the torque- or shear modulus and α a value of form elasticity. The elastic Modulus, the Poisson number and the Shear modulus are related by

$$\frac{E}{2G} = 1 + \mu. \quad \text{Eq. 9}$$

When the limiting values of μ (0 to 0.5) are considered the interval for G is:

$$\frac{E}{2} > G > \frac{E}{3}. \quad \text{Eq. 10}$$

2.2.2.2. PLASTICITY

In opposition to elastic behaviour, plasticity is the so-called irreversible material deformation. Plasticity depends on the loading path. [Error! Reference source not found.](#) s hows a stress-strain diagram for a material first undergoing elastic and then plastic deformation, leading up to material failure.

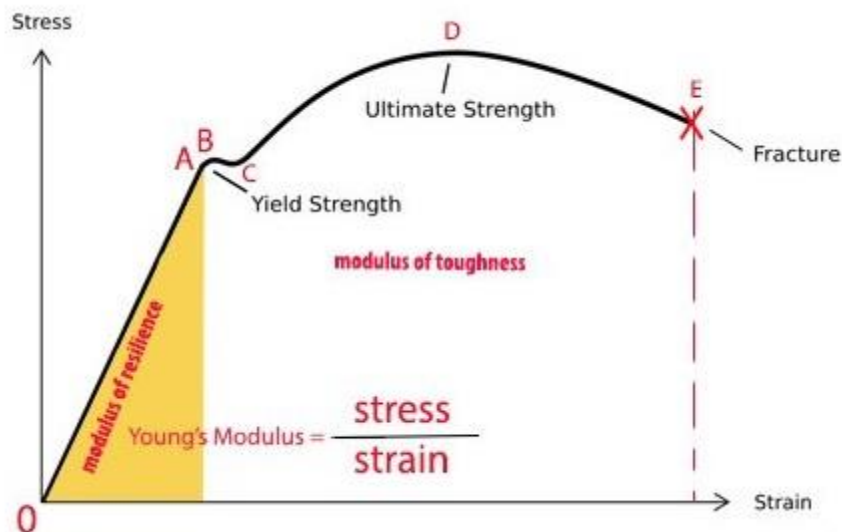


Figure 2-2. Stress-strain diagram of steel. First the steel is deforming elastically (linear region), then plastic deformation takes place. The Yield strength resembles the elastic limit. Up to this point the bar behaves linear elastic. After reaching the yield strength, strain increases more in comparison to the inflicted stress. When the stress would be released, purely elastic materials change back to their original shape. Past the yield strength, plastic deformation starts. All strains past this point are irreversible. The yield strength usually starts with plastic deformations and sudden hardening. At C is the breaking point. It is the highest strain a material can withstand. Further strain leads to a constriction in diameter and a loss in stress. The last point is the breaking point. The material fails and breaks apart.

The history of inflicted strains impacts the behaviour of the material. Plasticity occurs through rearrangements of molecules and structural changes within the material. Brittle

materials have no or just very little plasticity. Ductile materials exhibit plastic behaviour when inflicted stress and strain exceed the elastic behaviour.

2.2.2.3. VISCOSITY

Finally, I will introduce viscosity. It is the resistance of a fluid to deformation under a given stress. Fluids have neither a shape nor a memory of previous states. The stress within the fluid depends solely on the distortion speed of the molecules within. The inner movement of a fluid is determined by its inner friction. This friction is the result of reciprocal movement of molecules in neighbouring layers within the liquid. Viscosity η is defined as

$$\tau = \eta * \frac{dv}{dn} = \frac{F}{A}, \quad \text{Eq. 11}$$

with τ shear stress is force per area, or the dynamic viscosity times the gradient in speed. The inflicted force in between the neighbouring layers is evoked by the speed of the movement. Therefore, viscosity is unlike elasticity time dependent. High viscosity implies a high force that is needed to move the molecules in opposite direction. A sample with a high viscosity seems thicker than a material with a lower one

2.2.2.4. VISCOELASTICITY

A viscoelastic material shows a combination of elastic and viscous behaviour. When deformed, a fraction of energy is stored through the elastic behaviour, while the other fraction dissipates as viscosity. The so-called dynamic Modulus (also called complex Modulus) is used to describe this behaviour:

$$G = G' + iG'', \quad \text{Eq. 12}$$

G' is the elastic modulus (storage Modulus), while G'' is the loss modulus, which summarizes viscous effects. The contributions of both moduli depend on the frequency of the performed measurements. Viscoelastic stress-strain curves exhibit a hysteresis when the stress decreases. The area of the hysteresis is the dissipated energy. For the measurements in this work the evaluation of the elastic modulus is sufficient most of the time, for the acting force acts normal to the surface.

2.2.2.5. POROELASTICITY

The concept of poroelasticity finds large applicability in soil-sciences. Stones, pebble, and sand is the solid phase while water is the fluid. The idea of poroelasticity is useful to describe hydrogels and rubber for they reveal a similar behaviour.

It is basically a combination of all reactions of a solid porous material that is surrounded by interstitial fluid. The size of the pores limits the flow of the fluid and thereby defines the viscous properties. Thus, diffusion plays a key role, for it is the limiting factor for a change in shape.

2.2.2.6. SOFT-GLASSY RHEOLOGY

Soft glassy rheology is basically a “function of the mean values” of all energy state changes [56]. Particles are trapped in the energy landscape. When external energy impacts a body, the particles arise from these energetic traps and relocate in other meta states reaching a more stable state. Power Law Rheology models are the ones that are based on soft glassy rheology theory.

2.2.3. MATERIAL MODELS

Every material is described by its properties. Properties as such can be on a biological, chemical, and physical nature. A gel for instance may be a good incubator for bacterial life, it reacts with certain substances, with others not. Most people recognise a gel-like substance per touch. With stress-strain-time measurements mechanical properties can be derived that show the same “gel-like” behaviour as the real thing. Stress-strain curves can therefore be used to determine mechanical properties of materials. The relevance of mechanics is broad. Whether it is behaviour of a bridge to an earthquake, or a cartilage cell of a boar, there are certain similarities. Both resist stress and strain to stay intact. While the bridge needs maintenance, the cell adapts to the stress. In this section I will introduce various elastic and viscoelastic models used to describe the mechanical behaviour of biological materials.

2.2.3.1. SPRING, DASHPOT AND THE SAINT VENANT ELEMENT

Material mechanics can be described in simplified ways by using spring – dashpot – St. Venant elements. These elements can be combined in any number and configuration, including serial or parallel arrangements. The limiting factor for these models is the number of the unknowns. The spring represents the elastic proportion, as the dashpot accounts for the viscous part, and the St. Venant implies friction. In this thesis, only springs and dashpots will be considered.

2.2.3.2. HOOKE ELEMENT

For the Spring, also known as Hooke’s element, inflicted stress and strain happen immediately and are time independent. The deformation is limited and proportional to the

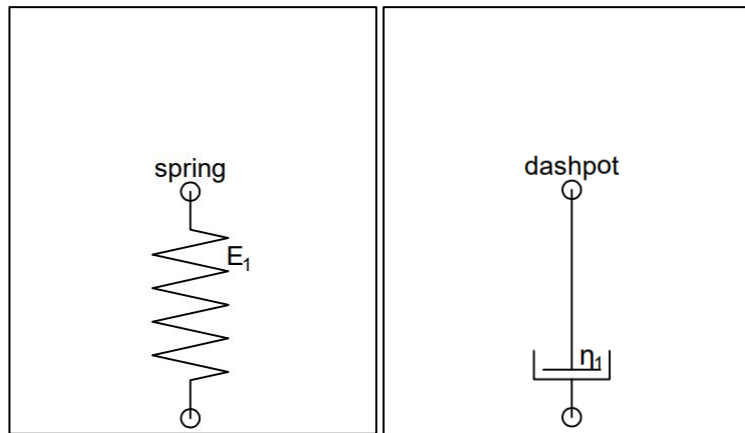


Figure 2-3. (Left) Representation of spring with a defined Young's Modulus. (Right) Representation of a dashpot with a defined viscosity.

inflicted stress. After loading, it returns to its original state in an instant. The spring represents an idle solid with a purely elastic response.

2.2.3.3. DASHPOT

The dashpot, or newton element, slows down the motion and dissipates energy via viscous friction. Instant strain is not possible for dampers. The viscous proportion is time dependent, and therefore also frequency dependent. The dashpot accounts for Newtonian liquids. The stress-strain relation of a Newtonian dashpot is

$$\varepsilon(t) = \frac{\sigma_0}{\eta} * t. \quad \text{Eq. 13}$$

2.2.3.4. MAXWELL ELEMENT

Maxwell aligned the spring and dashpot in series to account for viscoelasticity. Under load the Hooke-element deforms in an instant, after which the time-independent and unlimited viscous deformation begins. When the load is released, merely the spring moves back into its original state, the damper remains deformed. The time-dependent viscoelastic properties can be investigated using either creep (constant stress) or stress relaxation (constant strain) experiments. For creep, the stress-strain relation then is

$$\varepsilon(t) = \varepsilon_0 \left(1 + \frac{t}{\tau} \right), \quad \text{Eq. 14}$$

while for the case of stress relaxation it becomes

$$\sigma(t) = \sigma_0 * e^{\frac{-t}{\tau}}, \quad \text{Eq. 15}$$

where τ is the relaxation time, relating a Modulus with the viscosity.

2.2.3.5. KELVIN-VOIGT ELEMENT

In comparison to the Maxwell Model, Kelvin and Voigt put the spring and dashpot in a parallel configuration. The strain is distributed evenly, while the stress differs between each element. This model does not grand instantaneous deformations for at t_0 the strain is zero due to the time dependency of the damper. The spring can only deform the same amount as the dashpot. Under creep conditions, the stress-strain relation for a Kelvin-Voigt-Element is

$$\varepsilon(t) = \left(\frac{\sigma}{E}\right) * \left(1 - e^{-\frac{t}{\tau}}\right) \quad \text{Eq. 16}$$

A Kelvin-Voigt-element does not show stress relaxation, as the stress is taken up by the spring element and there is no relaxation over time.

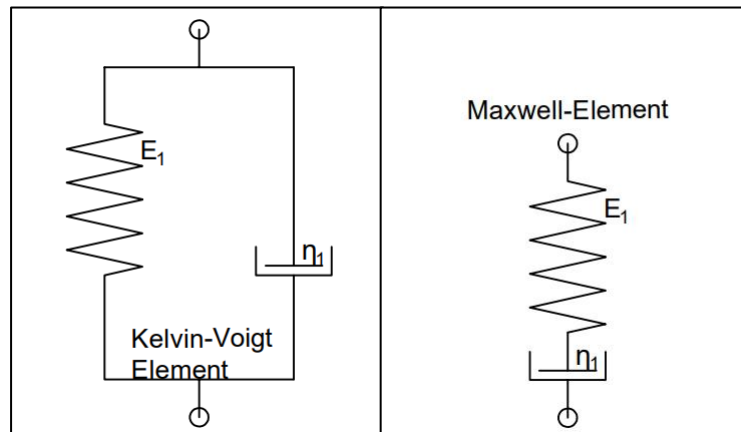


Figure 2-4 Kelvin-Voigt and Maxwell elements.

2.2.3.6. ZENER

The Zener model is also known as the Standard Linear Solid Model. It combines the Maxwell and the Kelvin Voigt models. Zener models are three-element models. There are different forms of the Zener models, depending on the arrangements of the springs and dashpots. Test most often used case in biological material mechanics is the standard linear solid with a Maxwell arm in parallel to a spring.

The Zener_m model is used to describe the creep of a material, while the Zener_k applies for stress relaxation. The creep response is defined as

$$\varepsilon(t) = \left(\frac{\sigma_0}{E_1}\right) * \left(1 - \frac{E_2}{E_1 + E_2}\right) * e^{-\frac{t}{\tau}} \quad \text{Eq. 17}$$

And the stress relaxation function is defined as

$$\sigma(t) = \varepsilon_0 * \left(E_1 + E_2 * e^{-\frac{t}{\tau}}\right). \quad \text{Eq. 18}$$

2.2.3.7. POWER LAW

A power law is an empirical fitting of a power function on a curve. For experimental relaxation and creep data, power laws provide good fits. The main disadvantage is that it does not show any characteristics of the relaxation time. Power laws are most often used in theories of soft glassy rheology. In addition, the complex shear modulus follows a weak power law behaviour in dependence of the frequency of the measurement [57].

2.3. ATOMIC FORCE MICROSCOPY IN BIOMECHANICS

The Atomic force microscope (AFM) is part of the scanning probe microscopes [58]. The measurement principle is that a cantilever is subjected to interactions with a surface and is therefore bending. Depending in whether the interactions with the surface are attractive or repulsive, the cantilever either bends toward or away the surface [59]. In analogy, it allows its user to “touch” a specimen. This therefore enables the user to not only determine sample surface topographic properties, but also to investigate mechanical, chemical, and electrical properties of the studied material.

Cantilevers are provided on macroscopic chips and are fixed onto the AFM glass head using a screw, a metal clamp or glue. Cantilevers come in different sizes and shapes. The tip end of the cantilever is the part of the AFM that undergoes contact with the specimen. When it meets the sample, repulsive forces lead to a bending away that leads to deflection of the beam. The bending of the beam is measured indirectly through a laser beam by a photodiode. The laser hits the beam and is reflected on the photodiode, which is divided in quadrants. Therefore, a voltage signal is the output of the measurement.

Within the AFM lies a piezoelectric element crystal. The characteristic of a piezo element is to change its length according to the strength of the applied electric current. Depending on the properties of the piezoelectric element, the change in length occurs on a sub nanometer scale. The piezo is used together with a feedback mechanism to tightly control the lateral and vertical positioning of the cantilever. It is one of the elements that determines the spatial, force and time resolution of the system.

The AFM's performance depends significantly on the right choice of the cantilever. Biological materials tend to be soft and sticky, and often organization at the nanoscale determines their properties. For these types of materials, the user often wants to investigate the sample with pN force resolution while still maintaining the nanometric spatial and the ms temporal resolution. Therefore, cantilever properties are highly important. A sensitive cantilever has to be as soft as possible but sensitive enough against the thermal energy,

while on the other hand it has to be able to react at reasonable timescales in the measurements.

The two most important values are the spring constant or likewise, the resonance frequency. The spring constant determines the stiffness and hence the bending resistance of the cantilever. The spring constant depends on the material of the cantilever (Young's Modulus) and its shape. Normally used cantilevers are in the range of a few hundred micrometers. As a rule of thumb, to produce a soft cantilever with the appropriate sensitivity, it should be both long and thin. In addition, cantilevers have reflective backside coatings to enable the photodiode detection. The cantilever stiffness has to be of similar scale to the order of the sample, otherwise either the sample will be deformed too much or only the cantilever is deformed during the measurements. Thus, choosing the right cantilever is crucial for measurement. The beams bending resistance should be slightly stiffer than the deformability of the specimen. In the case of cells, the spring constant for cantilevers is ranging in between 0.1 and 0.6 N/m.

In AFM measurement the definition of the contact area is crucial for the processing of the data. The contact area is defined by the geometrical shape of the tip and the shape and the behaviour of the specimen. The deliberation which tip serves the need, is a vital one. Tip shapes exist in any variation. The most common are sharp, spherical, cylindrical or plane cantilevers, which additionally vary in radius, diameter and length. A sharper tip leads to a higher spatial resolution and a deeper indentation. During this study, both a sharp nanometric tip and a μm -sized particle were used as indenters.

3. MATERIALS AND METHODS

3.1. AGAROSE GEL PREPARATION

Agarose gels of different concentrations (0.5 and 1.5 w/v%) were used to study the influence of loading rate on measured mechanical properties of hydrogels. Agarose granular was mixed with MilliQ water in two concentrations, 0.5% and 1.5% mass fraction agarose. The solvents were heated to 96°C in a microwave and poured into 30 mm diameter petri dishes to prepare gels of a thickness of a few millimeter. The gels were covered with MilliQ water to prevent the surface layer from drying. Prior to measurements, gels were stored in liquid at 4°C. Before AFM measurements, gels were removed from the freezer and kept at room temperature. Gels were measured by AFM in the Petri dish in MilliQ H₂O.

3.2. CELL CULTURE & SAMPLE PREPARATION

3.2.1. CELL CULTURE ROUTINE

MCF-7 epithelial breast cancer cells were a gift from Dr. Maria dM Vivanco (CIC bioGUNE, Bilbao, Spain). These cells are a model cell line for epithelial breast cancer. Cells were cultured under sterile conditions and all procedures were performed in a laminar hood (Herasafe KS12, Thermo Fisher Scientific). All disposable materials used were either purchased sterile or sterilized by autoclaving.

The cells were routinely cultured in DMEM with stable glutamine and high glucose content of 4.5 g/L. The media were supplemented using 10% fetal bovine serum and 1% mixture of penicillin and streptomycin (all purchased from Thermo Fisher Scientific). Prior to culturing, cells were stored in the gas-phase above liquid nitrogen, using the same medium with additional 10% DMSO. Cells were then thawed, re-suspended in the culture medium, and plated on T75 cell culture flasks (Sarstedt, Germany) at 37 °C, 5% CO₂ concentration and 95% humidity. Cells were routinely passaged every two to three days at a confluence of 80%, using passage relation of 1:5. A micrograph of the cells can be seen in **Figure 3-1**.

To passage the cells, they were first washed once with phosphate saline buffer (1X PBS, pH 7.4). Then, TrypLE™ was added and cells were incubated for 10 minutes at 37 °C. The suspension was diluted with 5 mL culture medium and centrifuged at room temperature for 5 min at 1200 rpm. The supernatant was discarded and the pellet dissolved in 5 mL culture medium. Then, 1 mL of the suspension was added to a T75 flask and 10 mL of culture medium were added. The flask was then put into the incubator.

During routine culture and for AFM sample preparation cells were counted and viability was checked using an automated cell counter (Countess® Cell Counter). Of the 1:5 diluted cell suspension, 10 μ L were mixed 1:1 with trypan blue (0.4%, Thermo Fisher Scientific), staining for dead cells. Cell viability was more than 90% during the study time. A maximum passage number of 40 was used.

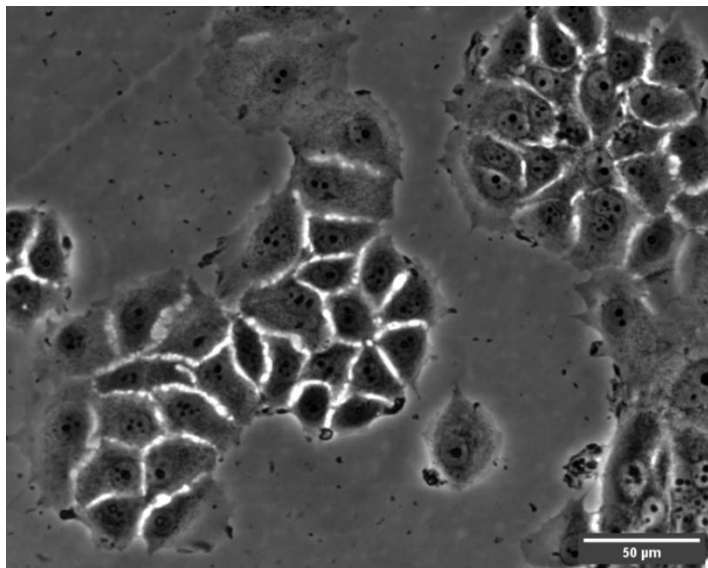


Figure 3-1. Micrograph of MCF-7 cells grown for 24 hours on glass slides in the culture medium. The image was done in phase contrast microscopy mode, with a 20x air objective.

3.2.2. SAMPLE PREPARATION FOR AFM MEASUREMENTS

Thin, circular (24 mm diameter, 0.4 mm thickness) glass slides (Menzel Gläser, VWR) were rinsed multiple times with ethanol and then dried with nitrogen. In a next step, they were cleaned by oxygen plasma (Gala Instruments, Germany) for 1 min at 50 W and a flow rate of 100 cm^3/min to remove all organic contaminations and activate the surface (making it more hydrophilic). Then, 1 mL of a cell suspension with a concentration of 100,000 cells/mL was added to the slide and diluted 1:1 with culture medium. The slides were incubated for 24 hours and, prior to AFM measurements, washed multiple times with PBS. Finally, CO_2 independent Leibovitz medium without any additional supplements was added.

3.3. BACTERIAL CULTURE & SAMPLE PREPARATION

3.3.1. BACTERIAL CULTURE

Escherichia coli BL21 DE3 strains were used for measuring bacterial mechanical properties. These are gram-negative, rod-shaped bacteria of the Enterobacter order and micrometer sized. Cultures were stored at $-70\text{ }^\circ\text{C}$ in LB medium with 10% glycerine. Of the storage cultures, one mL was added to inoculate 10 mL of LB medium and the culture was grown

overnight at 37 °C on an orbital shaker. Of the bacterial suspension, 1 mL was centrifuged at 12,000 rpm for 5 min on a table-top Eppendorf centrifuge, the supernatant was removed and the pellet resuspended in 1 mL 1X PBS at a pH of 7.4.

3.3.2. SAMPLE PREPARATION

Thin, circular (24 mm diameter, 0.4 mm thickness) glass slides (Menzel Gläser, VWR) were rinsed multiple times with ethanol and then dried with nitrogen. In a next step, they were cleaned by oxygen plasma (Gala Instruments, Germany) for 1 min at 50 W and a flow rate of 100 cm³/min to remove all organic contaminations and activate the surface (making it more hydrophilic). Then 1 mL of 0.2% PEI solution was added to the glass slides and they were incubated overnight at room temperature. Polyethylenimine is a strong poly-cation in aqueous solution, so bacteria will stick to the glass slide as the bacterial surface is negatively charged. After this step, the glass slides were rinsed three times with PBS. The re-suspended pellet was diluted 1:20 in PBS, 1 mL of the suspension was added to each glass slide and incubated for 1 hour at room temperature. The slides were then rinsed three times with PBS and kept in PBS prior to measurements.

3.4. CANTILEVER PREPARATION

As the three studied biological materials all have different sizes and mechanical properties, different cantilevers were applied in the mechanical measurements. summarizes the properties of the three different cantilevers.

Table 3-1. Cantilevers used to study the three different biological materials (gels, cells and bacteria).

Cantilever	Spring Constant [N/m]	Frequency [kHz]	Shape	Tip radius
FORTG-TL	1.6	61	Rectangular	5 µm
NP-O, B	0.12	23	Triangular	5 µm
MSCT, E	0.1	38	Triangular	10 nm

For studying agarose gel mechanical properties, rectangular tip-less cantilevers (FORTG-TL, AppNano) were used. These were modified with silica particles as described below. For the cellular measurements, triangular tip-less cantilevers (NP-O, cantilever B, Bruker) were used and modified with particles. Finally, bacteria measurements were done using triangular cantilevers with a pyramidal tip (MSCT, cantilever E, Bruker). Prior to measurements, cantilevers were cleaned for 1 hour by UV/O cleaning. After measurements, cantilevers were cleaned using series of water/EtOH cleaning. **Figure 3-2** shows scanning electron microscopy images of cantilevers.

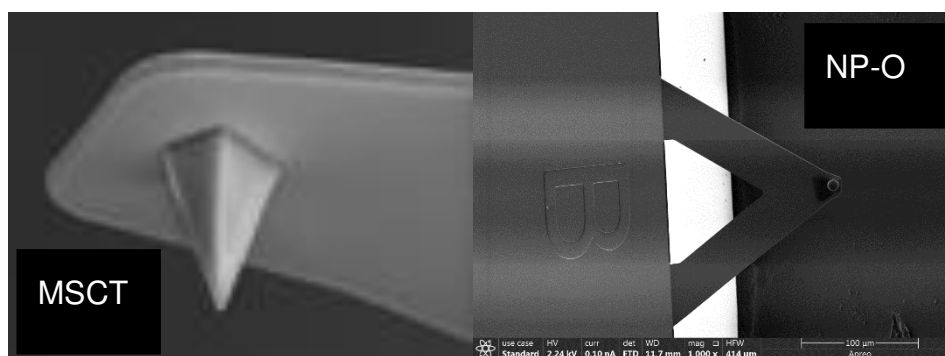


Figure 3-2. Scanning Electron Microscopy Images of Cantilevers used in this study. (Left) MSCT tip (taken from manufacturer website). (Right) NP-O cantilever after particle glueing.

3.4.1. PARTICLE GLUEING

To glue a microbead to the cantilever needs some preparation. The following steps were applied for setting up the cantilever. Microscopy glass slides were prepared for the plasma cleaner by cleaning them with microfiber tissues, water, and ethanol. They were dried in nitrogen and then plasma cleaned as the glass slides described above. Then, a drop of UV-curable glue (Norland Optical Adhesive, NOA68) was added to a glass side and pulled into thin lines with the tip of a pipette. Then, a tip-less cantilever was fixed to the AFM Nanowizard III head and a glue drop was carefully approached by the end of the cantilever using the stepper motors. The cantilever was then used to touch the glue with a feedback loop for 5 s and retracted again to break up the contact.

The next step was to pipette a diluted suspension with silica microbeads of 5 μm radius (Microparticles, Germany) on another cleaned glass slide. Then, the cantilever was brought into contact with the liquid and a particle was approached using the stepper motors. Using the microscope and the x- and y-motion of the AFM piezo, the cantilever was positioned above a particle and brought into contact until maximum deflection was reached. The cantilever was left in contact with the particle for 10 s, then retracted for 200 μm using the stepper motors, and a successful adhesion of a particle to the glue was checked using the

microscope. The glue was then cured using a UV-light at 380 nm for 10 minutes. Then, the cantilever was removed from the solution, cured for 30 minutes more in air and a final curing step at 50 °C was done in an oven. **Figure 3-3** shows a FORTG cantilever and a NP-O cantilever with particles.

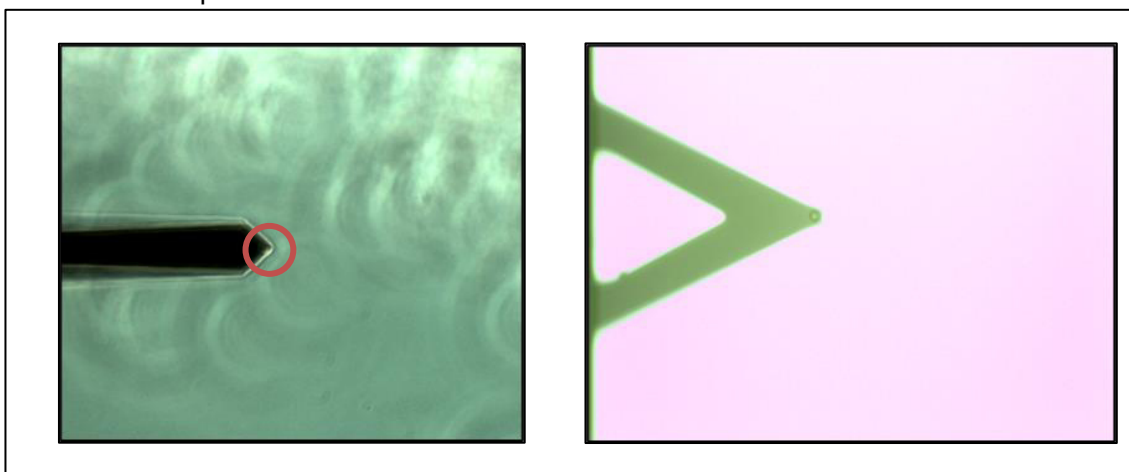


Figure 3-3. Cantilevers after the particle gluing step. (Left) FORTG cantilever with 10 μm diameter particle. (Right) NP-O B cantilever with 10 μm diameter silica particle.

3.5. ATOMIC FORCE MICROSCOPY

A JPK Nanowizard III Atomic Force Microscope (JPK instruments, today Bruker, Germany) was used. The AFM was equipped with a CellHesion module (enabling measurements with a z-range of 100 μm), a Biocell® and a liquid sample holder. The instrument is combined with an inverted optical microscope (Axio Observer Z1, Zeiss) that is equipped with different objectives (10x phase contrast objective used in this study). Gel measurements were performed at room temperature in water in petri dishes, cell measurements at 37 °C in the cell sample holder in Leibovitz media and bacteria measurements at room temperature in a liquid sample holder. Prior to measurements, sample slides were added to the sample chamber, 500 μL of the buffer was added and the AFM head with the cantilever was added to the liquid. The system was then left for equilibration for 30 min in the sample buffer.

3.5.1. AFM CALIBRATION

Prior to AFM measurements, the cantilever had to be calibrated [60]. This is done to determine the sensitivity and stiffness of the cantilever. For this, the laser spot was focused on the end region of the cantilever and the occurring voltage signal was maximized. The cantilever of an AFM bends as a response to interactions between the tip and the sample. Those interactions can be either attractive (bending toward surface) or repulsive (bending away). The deflection of the cantilever in z-direction Z_c is modelled as an ideal Hookean spring by

$$F = k_c \times Z_c, \quad \text{Eq. 19}$$

where F is the force acting on the cantilever and k_c is the spring constant. To determine the spring constant and the sensitivity of the cantilever, first a force distance curve with 5 $\mu\text{m/s}$ and 2 V maximum deflection was performed on a stiff substrate (glass). As the substrate is “infinitely” stiffer than the cantilever, only cantilever bending is recorded. In a next step, the inverse slope of the contact region is determined, being the sensitivity of the system. Then a thermal noise spectrum of the cantilever is recorded by letting it vibrate freely. The equipartition theorem is used to determine the spring constant of the cantilever as

$$\frac{1}{2}k_c\langle Z_c^2 \rangle = \frac{1}{2}k_bT, \quad \text{Eq. 20}$$

which is reformed to

$$k_c = \frac{k_bT}{\langle Z_c^2 \rangle}, \quad \text{Eq. 21}$$

where k_b is the Boltzmann constant, T is the temperature and $\langle Z_c^2 \rangle$ is the mean squared displacement of the cantilever. This calibration method is called thermal tune.

3.5.2. FORCE SPECTROSCOPY

To determine the mechanical properties of the gels, cells and bacteria, so-called force-distance curves were recorded with the AFM. In this case, the sample was approached by the cantilever and indented, and then the cantilever was retracted again. The relationship of force to indentation can be used to calculate the elastic properties. To determine frequency dependent mechanics, measurements were performed with different loading rates.

3.5.2.1. GEL MEASUREMENTS

Two agarose gel concentrations (0.5 and 1.5 w/v%) were chosen to have a control measurement and to see whether the results are as expected that the gel with the lower concentration is softer and more liquid-like than the other. A measurement grid of 50 x 50 μm was set up and for each maximum force and approach rate 50 force-distance curves were measured. The measurement settings were done as can be seen in **Table 3-2** and **Table 3-3**. The data evaluation process is described later.

Table 3-2 Experiment setup for the 0.5% Agarose gel AFM measurements

0.5%		Curve Length		
Velocity	Sampling Rate	5 nN	25 nN	50 nN
$\mu\text{m/s}$	Hz	μm	μm	μm
0.25	1000	2.0	2.5	3.2
0.50	1000	2.0	2.5	3.2
1.00	1000	2.0	2.5	3.2
2.50	1000	2.5	2.5	3.2
5.00	10000	2.5	2.5	3.2
10.00	10000	3.0	2.5	3.2
25.00	20000	3.0	2.5	3.2

Table 3-3 Experiment setup for the 1.5% Agarose gel AFM measurements

1.5%		Z- Length		
Velocity	Data Points	5 nN	25 nN	50 nN
$\mu\text{m/s}$	Hz	μm	μm	μm
0.25	1000	1.0	1.0	1.0
0.50	1000	1.0	1.0	1.0
1.00	1000	1.0	1.0	1.0
2.50	1000	1.0	1.0	1.0
5.00	10000	1.0	1.0	1.0
10.00	10000	1.0	1.0	1.0
25.00	20000	1.5	1.5	1.5

3.5.2.2. CELL MEASUREMENTS

Living cells were measured in Leibovitz medium at 37 °C. The sample was measured for a maximum time of four hours to ensure that cells did not change properties over time. **Figure 3-4** shows a representative micrograph of how the cells together with the cantilever look like. The setup of the experiment was to measure each cell at 1 nN max force and at six

velocities (1, 2, 4, 8, 16, 32 $\mu\text{m/s}$). The length of the baseline was set 8 μm . The frequency of the recorded data points was raising with velocity (512 Hz at 1 $\mu\text{m/s}$, 1048 Hz at 2 $\mu\text{m/s}$ and 2048 Hz for the other measurements). 20 different cells were measured and each measurement was repeated 3 times.

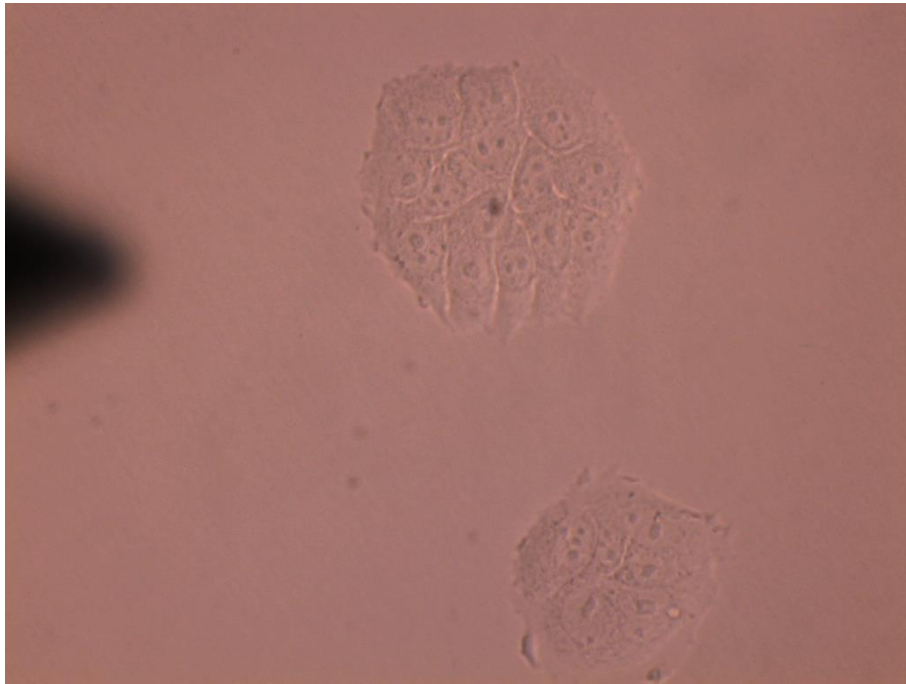


Figure 3-4. MCF-7 cells grown on glass slides for 24 hours. The black triangular shadow indicates the cantilever.

3.5.2.3. BACTERIA MEASUREMENTS

Figure 3-5 shows the measurement set-up for bacterial mechanical measurements. First, a 20 x 20 μm image was performed in QI mode to determine the location of the bacterial cells. Then, force maps were performed on at least 10 bacteria with 5 x 5 measurements. The length of the curves was 1 μm and the maximum load 1 nN. Measurements were done at loading rates of 0.5, 1, 2, 8, 16 and 32 $\mu\text{m/s}$. The sampling rate was set accordingly.

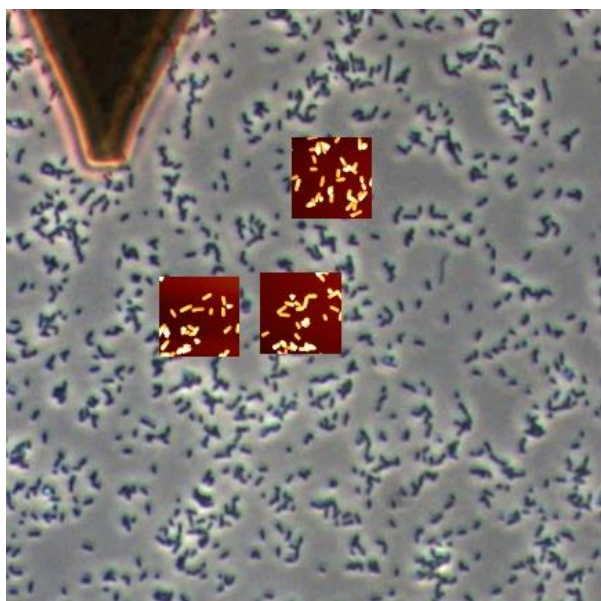


Figure 3-5. Phase contrast microscopy image of bacteria immobilized on PEI-coated glass slides. Top left corner shows the triangular end of the cantilever. The coloured insets show QI mode images of the bacteria.

3.5.3. DATA ANALYSIS

For the three different biological materials that were measured, similar data analysis steps were performed. A typical experiment consists of an approach curve that has two distinct parts: The baseline and the contact region (indentation of the sample). In contact, the contact between the cantilever end and the sample leads to a repulsion of the cantilever. Therefore, in a first step, the contact point must be determined.

In this thesis, this was done mostly by using the software provided by the AFM manufacturing company (JPK SPM software, JPK Instruments, Version 6.1.183). In addition, bacterial measurements were evaluated using a self-written package in R [61], [62]. Four simple data manipulation steps were performed. The steps were performed as can be seen in **Figure 3-6** and are described more in detail below.

- A batch of force distance curves is loaded into the software. In red the approach/indentation curve is shown, while the blue curve corresponds to the

retraction segment. There is a clearly indicated difference between the baseline and the contact segment. As both the approach and the retract part of the curve do not overlap, hysteresis can be seen.

- The baseline is defined as the region with no slope before the contact. Then the curves are tilted according to the baseline.
- The contact point is determined automatically by the software and is adjusted by eye as the region of the curve that has a difference in slope. In the R toolkit this is done by a different, novel algorithm.
- In the final step, the bending of the cantilever is corrected to determine the deformation of the sample.

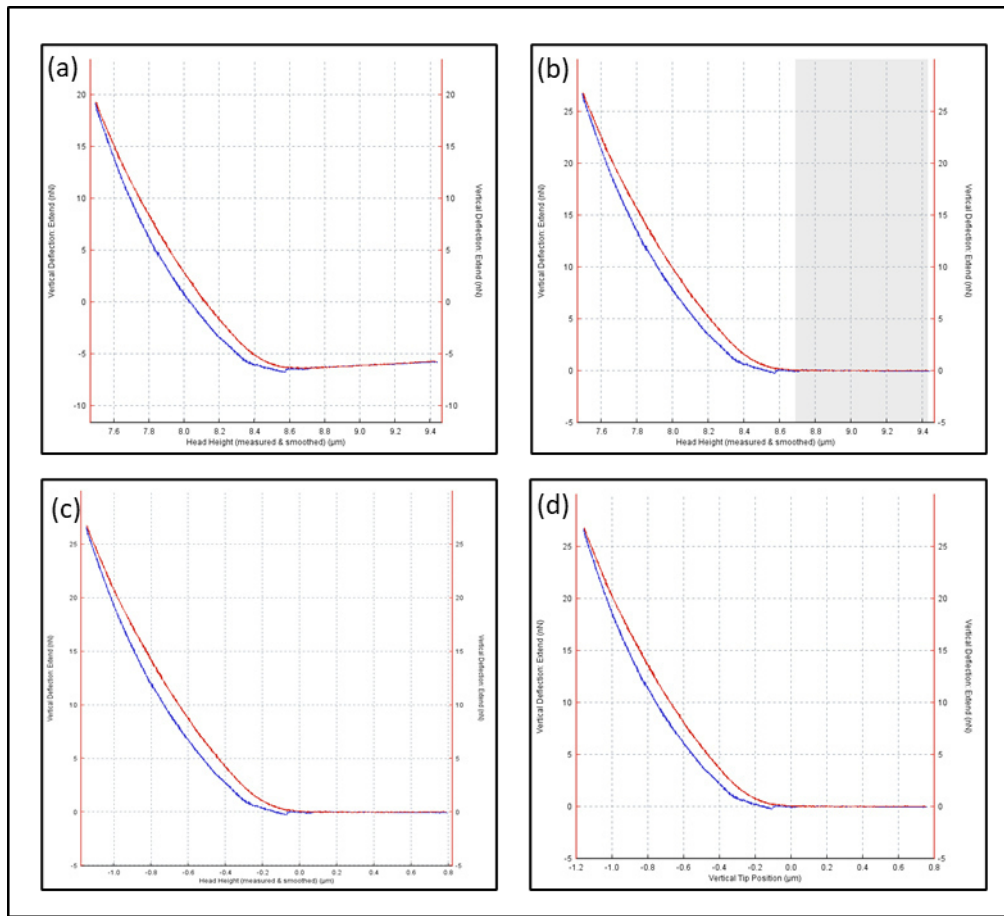


Figure 3-6. Curve manipulation steps. (a) Raw Force-distance curve, in red the approach and in blue the retract part can be seen. (b) Baseline correction. (c) Contact point definition. (d) Correction of cantilever bending.

In the AFM experiment, the distance D between the tip and the sample is defined as

$$D = Z_p - (\delta_c + \delta_s), \quad \text{Eq. 22}$$

where Z_p is the position of the piezoelement, δ_c is the deformation of the cantilever and δ_s the deformation of the sample. As defined above, the cantilever is thought to behave as

ideal elastic spring and therefore the cantilever deformation is determined by the force that is applied to it. Therefore, in contact with the sample (where we define the contact point), the deformation of the sample is

$$\delta_s = Z_p - \delta_c = Z_p - \frac{F}{k_c}. \quad \text{Eq. 23}$$

The data analysis was performed by batches and then the curves were extracted to ASCII files and further processed in OriginPro 2018 (OriginLab) or in R. Outlier curves were removed prior.

3.5.3.1. FORCE-DISTANCE CURVES ANALYSIS

For each sample, loading rate and maximum load, data sets were pooled, and Force-distance curves were plotted. Then, average curves were calculated. **Figure 3-7** shows the pooled curves for measurements on the 0.5% Agarose gel with a maximum load of 25 nN and a loading rate of 1 $\mu\text{m/s}$.

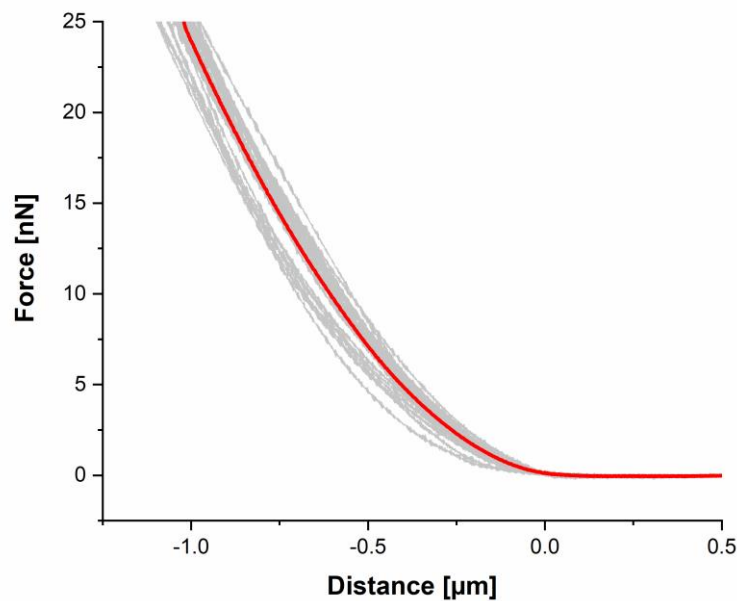


Figure 3-7. Pooled F-d-curves after the correction steps for measurements on a 0.5% Agarose gel with a 5 μm radius silica particle, a maximum load of 25 nN and approach velocity of 1 $\mu\text{m/s}$.

In this thesis, simple Hertzian elastic theory with the Sneddon extension for different indenter geometries was used. In principle, the application of force to a material leads to a deformation that follows the relationship

$$F = C \times \delta^i, \quad \text{Eq. 24}$$

where the constants C and i depend on the geometry of the system. For a parabolic indentation profile, the relationship is

$$F = \frac{4}{3} \sqrt{R_c} \frac{E_{sample}}{1 - \nu^2} \delta^{3/2}, \quad \text{Eq. 25}$$

where R_c is the radius of the parabolic indenter, E_{sample} is the apparent Young's Modulus (elastic Modulus) and ν is the Poisson ratio (set to 0.5 assuming incompressibility of the material). In literature, often the reduced Young's Modulus E' is shown as

$$\frac{1}{E'} = \frac{(1 - \nu_{tip}^2)}{E_{tip}} + \frac{(1 - \nu_{sample}^2)}{E_{sample}}, \quad \text{Eq. 26}$$

where the former term can be ignored as the elastic modulus of the tip (silica) is much higher than that of the samples investigated here. It is easily seen from the above relationship that by plotting F vs $\delta^{3/2}$ a linear relationship can be used to determine sample elastic properties. Reformulating the equation above leads to

$$E = \frac{3(1 - \nu^2)}{4} \frac{\Delta F}{\sqrt{R_c} \Delta \delta^{3/2}} = \frac{3(1 - \nu^2)}{4} \frac{1}{\sqrt{R_c}} \times S, \quad \text{Eq. 27}$$

where S is the slope of the linear fitting. For the three different samples, different indentation ranges were used to determine elastic properties This was done to test the validity of the elastic theory used. Bacterial measurements were solely evaluated using the R afmToolkit.

Finally, the resulting apparent Young's Moduli were pooled for the different loading rates and plotted against the loading rates. As there seemed to be a relationship between the value and the loading rate, I used a power law model to describe it [21]. The model followed

$$E(\omega) = E_0 \left(\frac{\omega}{\omega_0} \right)^\alpha, \quad \text{Eq. 28}$$

Where E_0 is the Modulus at rest, ω is the frequency, ω_0 a reference frequency set to 1 Hz and α is a power law exponent that ranges from 0 to 1. If it is 0, then the material behaves purely elastic solid, and if it is 1 it behaves as a pure viscous fluid. To simplify, instead of frequencies, loading rates were included in this analysis.

4. RESULTS AND DISCUSSION

In this chapter the results of the measurements are reported and discussed. The first subchapters deal with different measurements of the agarose gels, E. coli and MCF-7 cells. The comparison of forces may give an insight, whether the materials behave according to ideal elastic theory. A deviation from this theory can arise due to sample anisotropies. In addition, a comparison of the calculated elastic properties at different loading rates gives an indication about whether the sample behaves more like an elastic solid or like a viscous fluid.

4.1. AGAROSE GELS

In this chapter, the measurements performed on 0.5 and 1.5 % Agarose gels are discussed. Agarose is a simple hydrogel and the mechanical properties are determined by the Agarose content, which determines the amount of cross-linking in the gel.

4.1.1. FORCE DISTANCE CURVES

Figure 4-1 to **Figure 4-6** display the actual measurements performed by AFM in grey while the determined averaged force-distance curve is coloured in red. Measurements were done with loading rates of 0.25, 0.5, 1, 5, 10 and 25 $\mu\text{m/s}$ and maximum forces of 5, 25 and 50 nN. These measurements were performed using a spherical indenter with a radius of 5 μm . **Figure 4-1**, **Figure 4-2** and **Figure 4-3** show the measurements performed on the 0.5% Agarose gel, while **Figure 4-4**, **Figure 4-5** and **Figure 4-6** show the ones on the 1.5% gel. Overall, no increase of slope that would indicate an increase in the measured mechanical elastic properties can be seen. For the curves performed at similar conditions, the curve shapes appear similar. For the low concentration gel the average indentation is around 500 nm for a maximum load of 5 nN, 1 μm for 25 nN and 1.5 μm for 50 nN. For the 1.5% gel, the indentation is around 150 nm for 5 nN, 250 nm for 25 nN and 350 nm for 50 nN. The lower indentation at the same force for the higher concentrated gel indicates that it is stiffer than the low concentrated one. For all measurement sets an increase in noise can be seen at higher loading rates due to larger vibrations and increased hydrodynamic pressure.

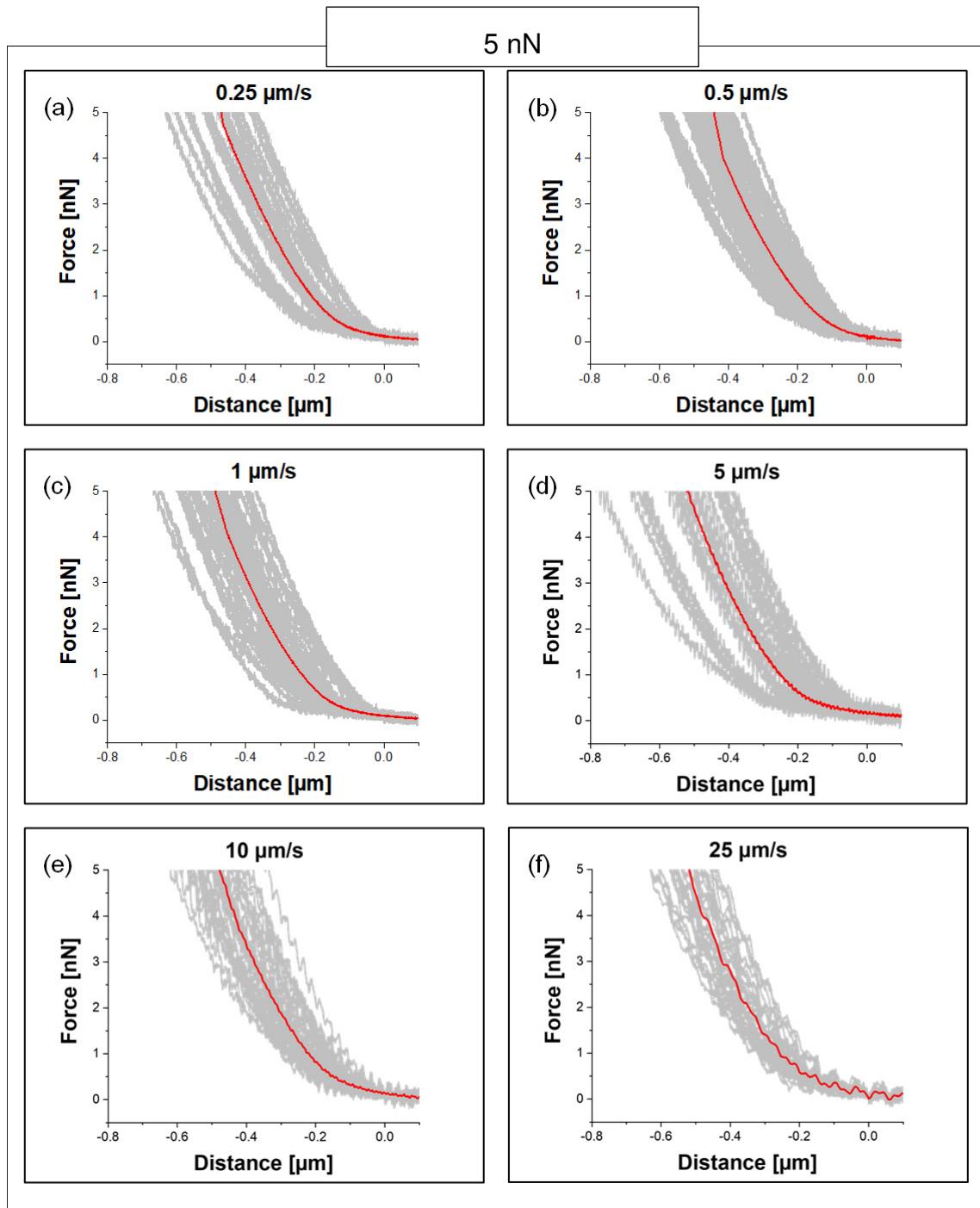


Figure 4-1. Force-distance-curves of 0.5 % w/v agarose gel measured with a spherical particle at a maximum load of 5 nN and with loading rate ranges from 0.25 to 25 $\mu\text{m/s}$. Grey lines indicate the measurement data, while the red lines show the averaged measurements.

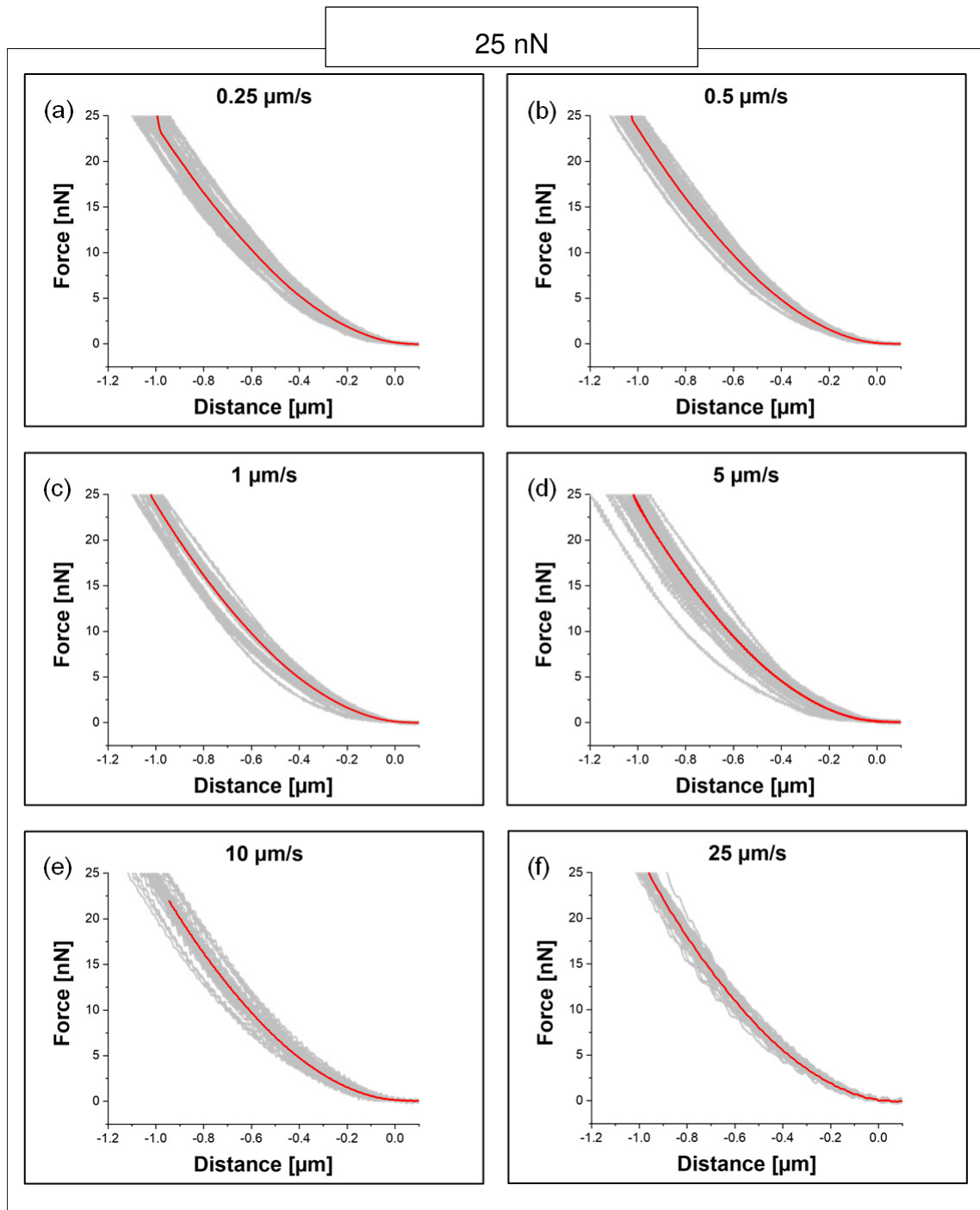


Figure 4-2 Force-distance-curves of 0.5 % agarose gel measured with a spherical particle at a maximum load of 25 nN and with loading rate ranges from 0.25 to 25 $\mu\text{m/s}$. Grey lines indicate the measurement data, while the red lines show the averaged measurements.

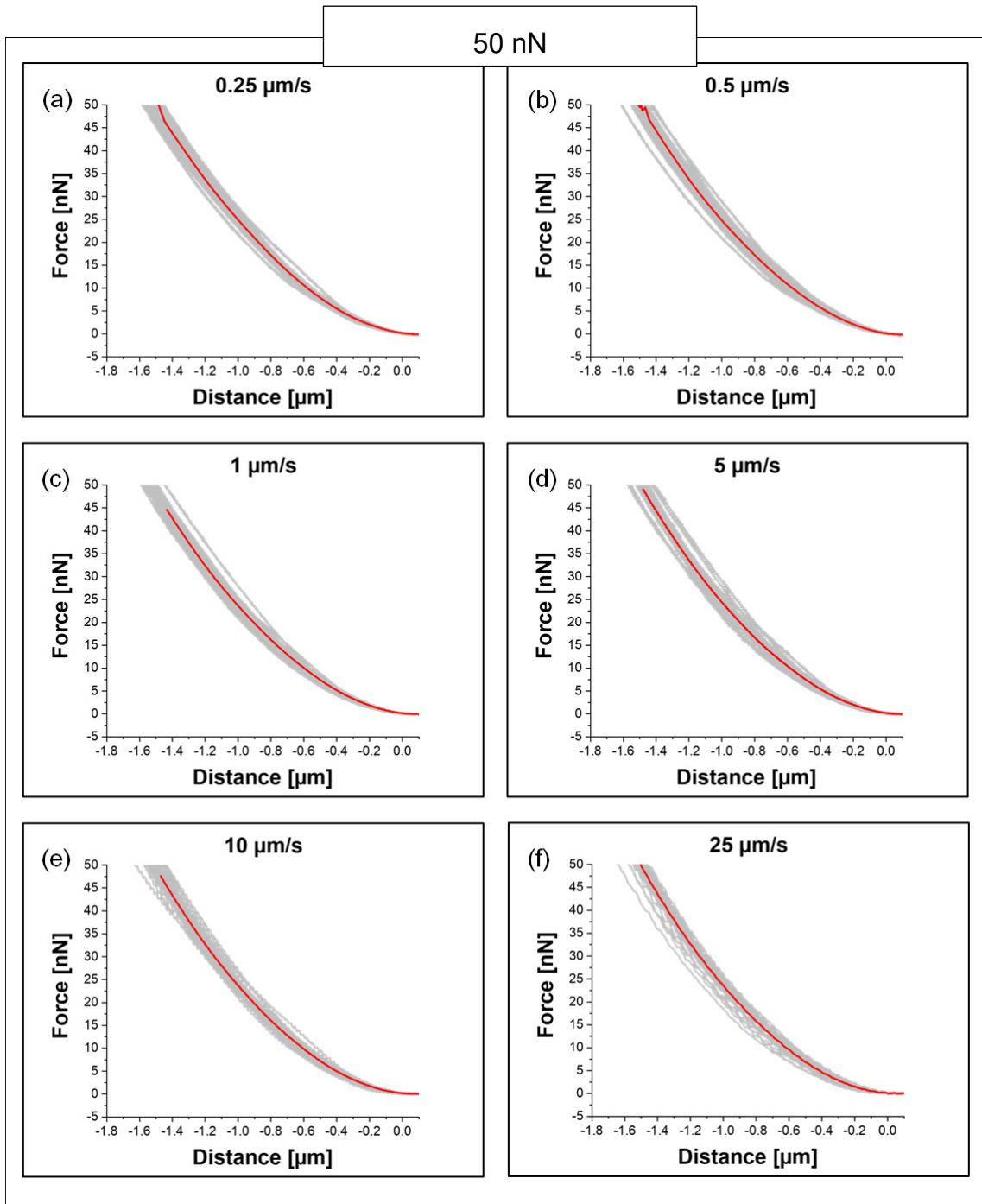


Figure 4-3 Force-distance-curves of 0.5 % agarose gel measured with a spherical particle at a maximum load of 50 nN and with loading rate ranges from 0.25 to 25 $\mu\text{m/s}$. Grey lines indicate the measurement data, while the red lines show the averaged measurements.

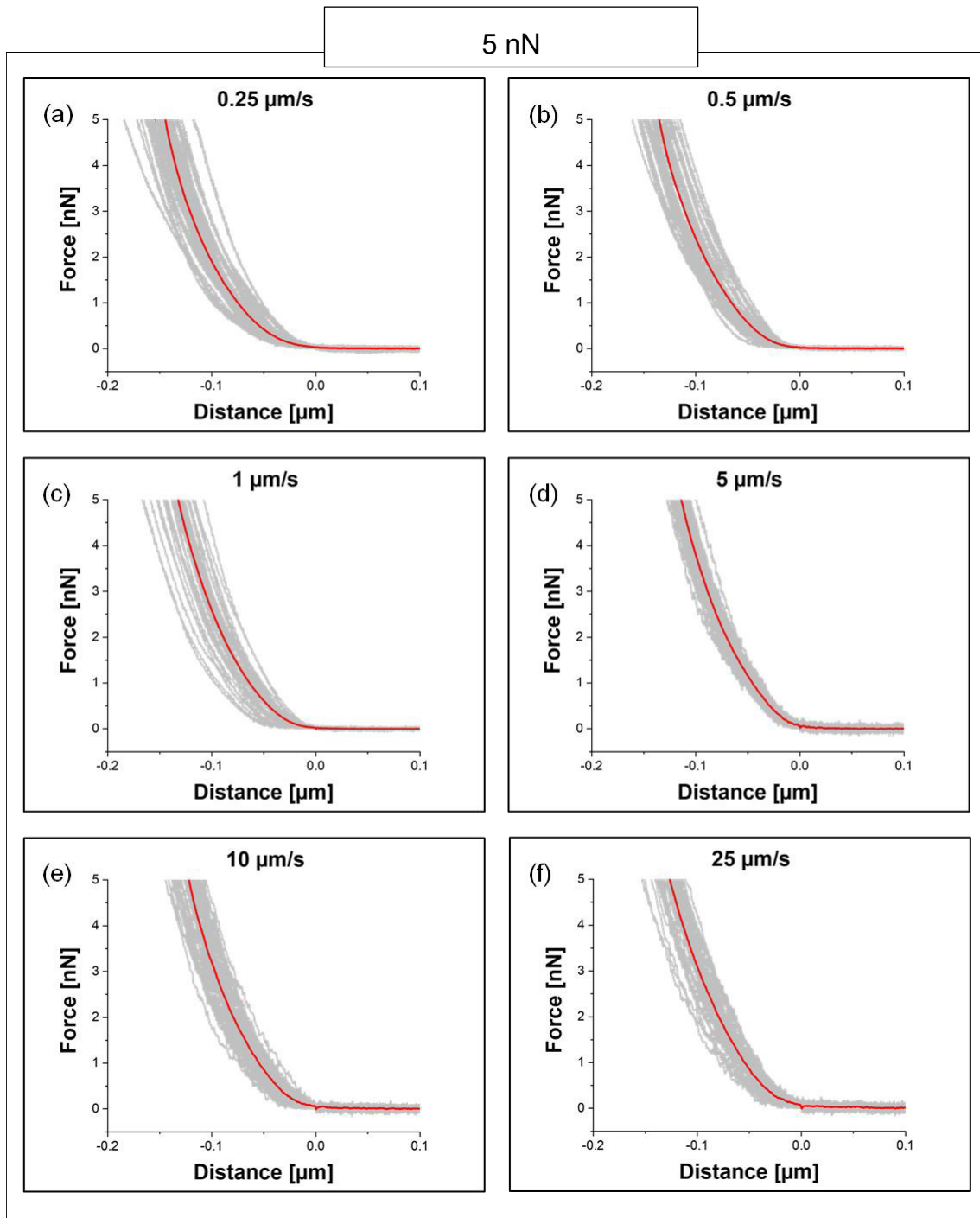


Figure 4-4 Force-distance-curves of 1.5 % agarose gel measured with a spherical particle at a maximum load of 5 nN and with loading rates ranges from 0.25 to 25 $\mu\text{m/s}$. Grey lines indicate the measurement data, while the red lines show the averaged measurements.

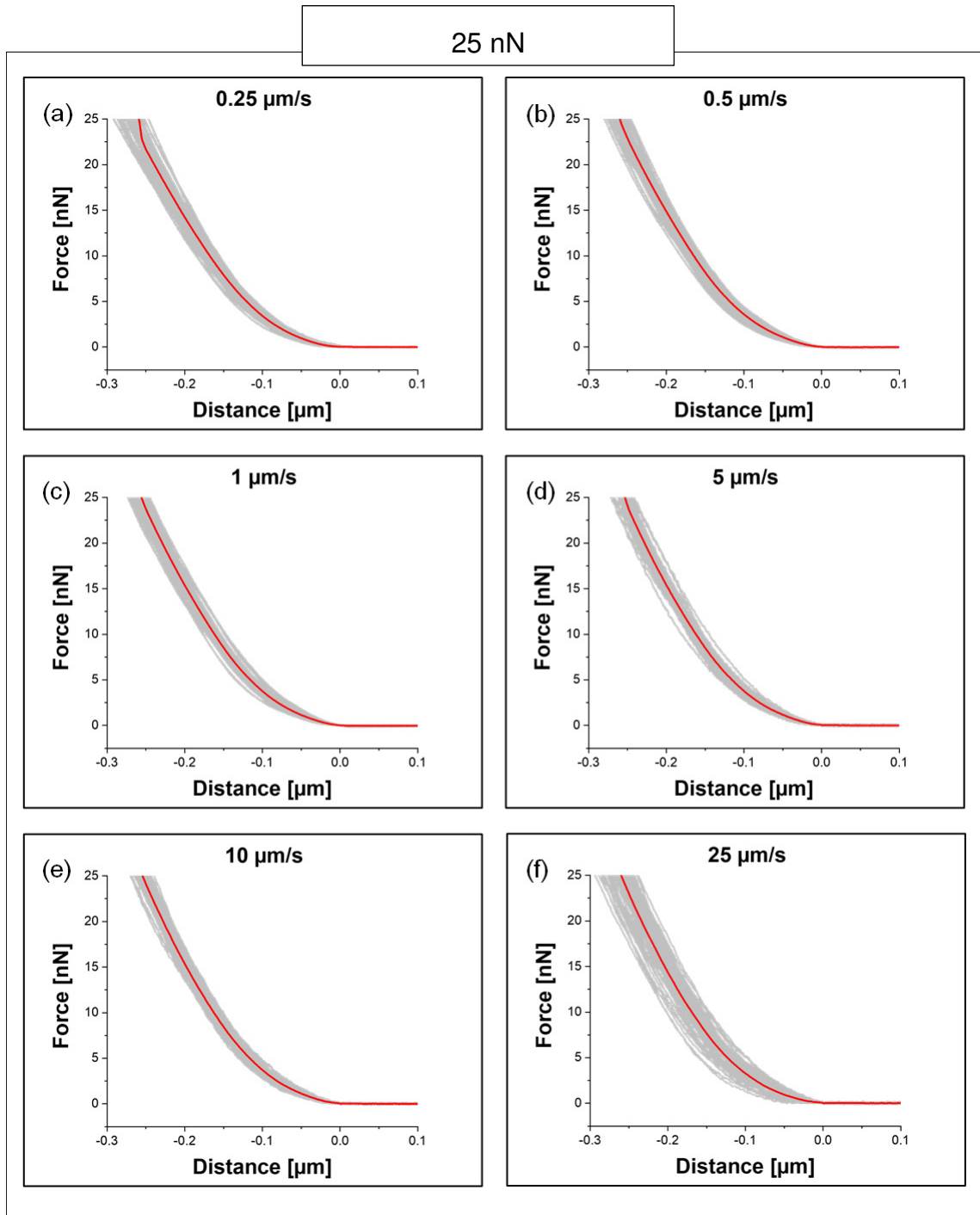


Figure 4-5 Force-distance-curves of 1.5 % agarose gel measured with a spherical particle at a maximum load of 25 nN and with loading rate ranges from 0.25 to 25 $\mu\text{m/s}$. Grey lines indicate the measurement data, while the red lines show the averaged measurements.

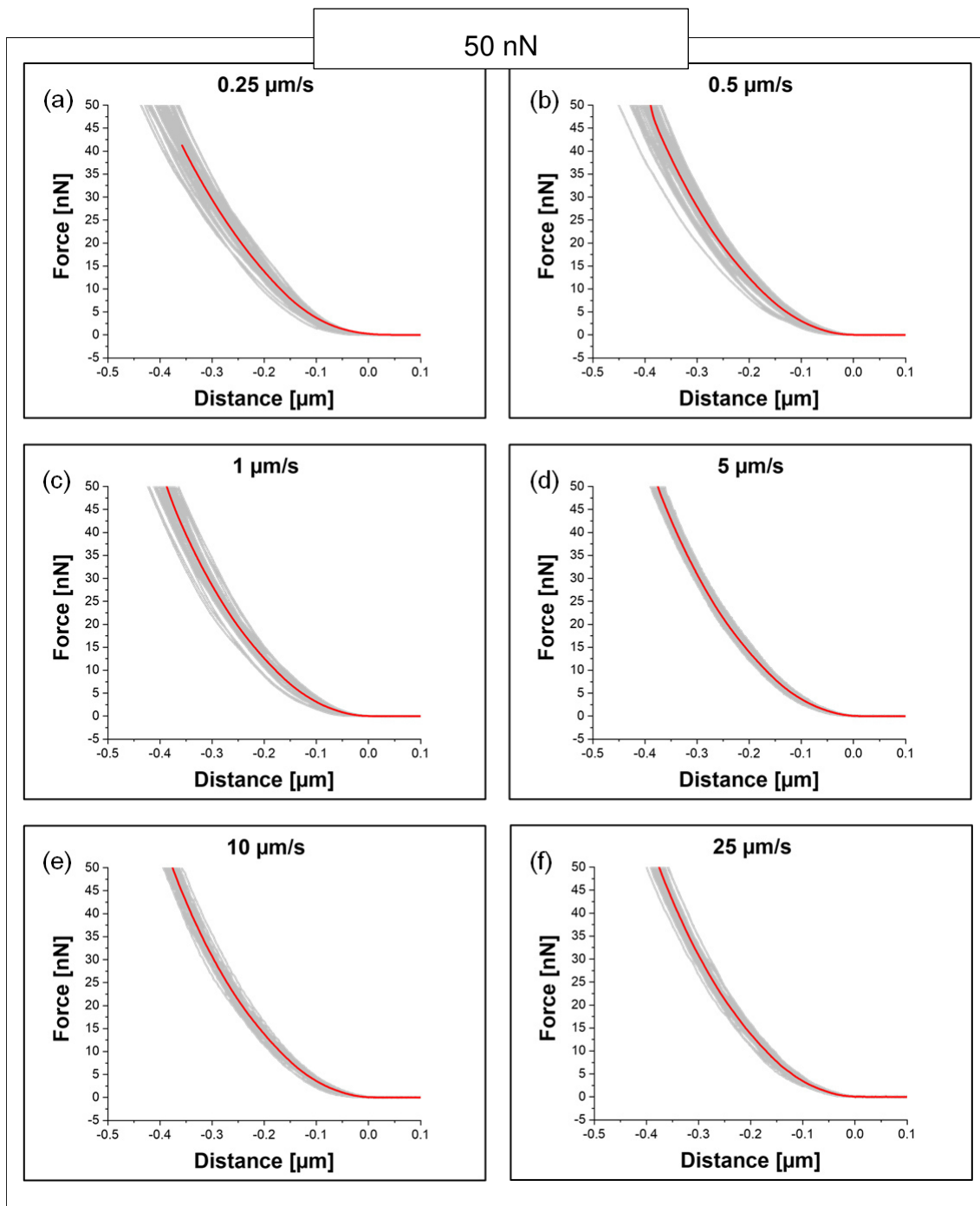


Figure 4-6 Force-distance-curves of 1.5 % agarose gel measured with a spherical particle at a maximum load of 50 nN and with loading rates ranges from 0.25 to 25 $\mu\text{m/s}$. Grey lines indicate the measurement data, while the red lines show the averaged measurements.

4.1.2. COMPARISON OF THE AGAROSE GEL CONCENTRATIONS FOR F-D CURVES

The averaged curves of the previous force-distance measurements were pooled together. This allows a better comparison of the slopes at different loading rates and different concentrations of gels with changes in the maximum load. This analysis can be seen in **Figure 4-7**. The rainbow colour coding is according to the increase in loading rate, from blue being 0.25 $\mu\text{m/s}$ to red being 25 $\mu\text{m/s}$. From these plots, no increase in stiffness with increasing loading rate is evident, especially not for the measurements performed at 25 and 50 nN. For the 5 nN measurements, random differences appear for the loading rates, which are attributed to larger relative errors that are made when averaging curves at lower indentations of a few hundred nanometres.

Summing up **Figure 4-7**, there does not appear to be much evidence for a viscous contribution to the mechanical properties of the hydrogels at the measured loading rates and loads. In comparison, the 0.5% and the 1.5% agarose gel behave similar, with the obvious exception in indentation depth due to the higher concentration of agarose, making these gels stiffer.

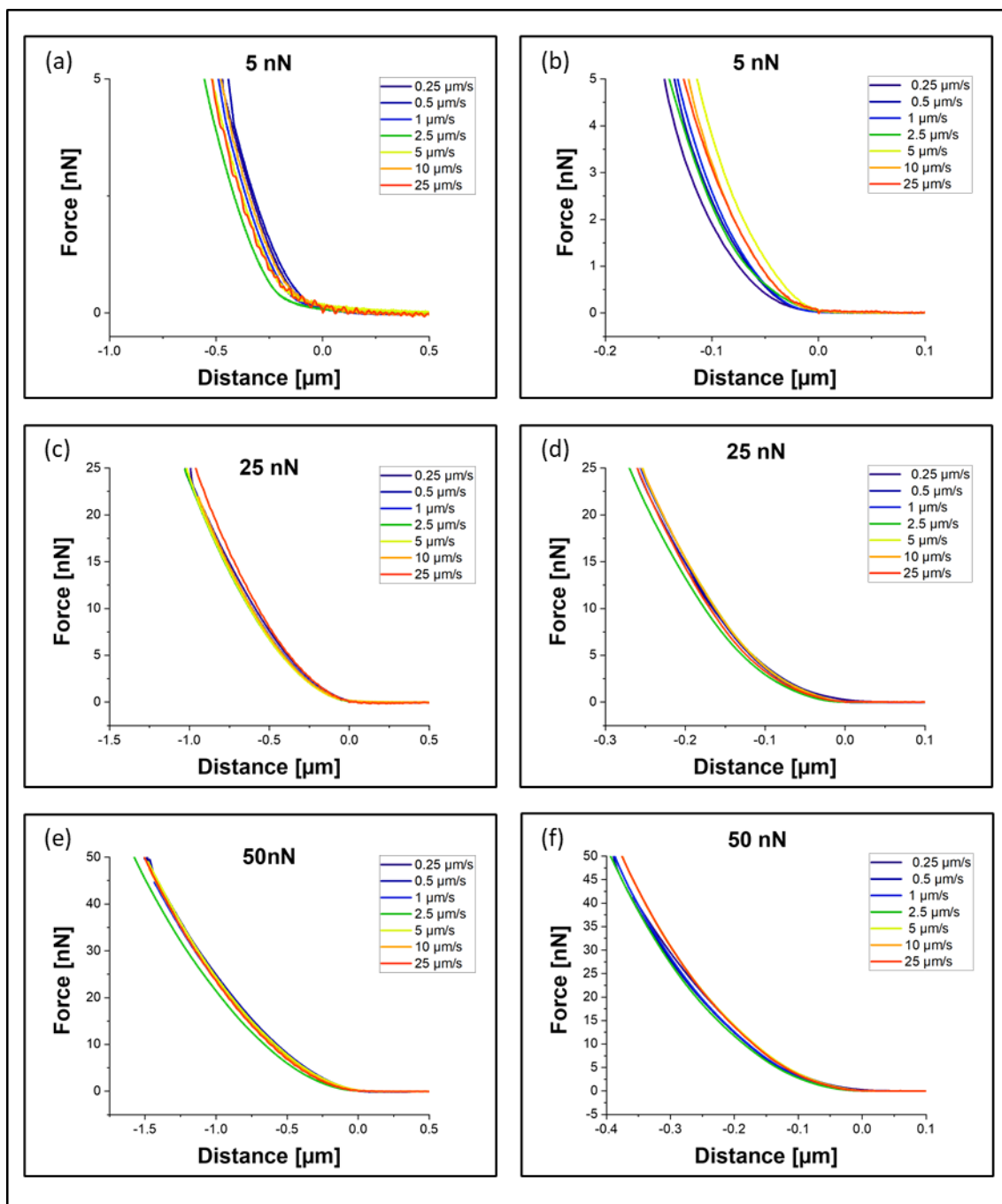


Figure 4-7 These curves show the averaged force-distance curves of the previous measurements. On the left side is the 0.5% and on the right side the 1.5% agarose gel. These curves were measured at 5, 25, and 50 nN and with loading rates ranging from 0.25 to 25 $\mu\text{m/s}$. The indentation differs by concentration of the gel. (a,c,e) from 0.5 μm to 1.5 μm and (b,d,f) 0.1 μm to 0.4 μm . Colour coding indicates the different loading rates. Note that the x-axis is scaled differently for the two different gels.

4.1.3. FITTINGS OF THE FORCE-DISTANCE^{3/2} CURVES FOR GELS

To determine the elastic Modulus of the gels, linear fittings of F vs $\delta^{3/2}$ were performed. From the determined slope, the Elastic Modulus can be calculated depending on the size of the indenter. The steeper the slopes, the stiffer the material, and therefore the higher the calculated Modulus is. **Figure 4-8** shows an example of such a fitting for a single curve. The fitting performs very well (R^2 of 0.998) and a Young's Modulus of 6.15 kPa can be determined for this specific measurement and sample.

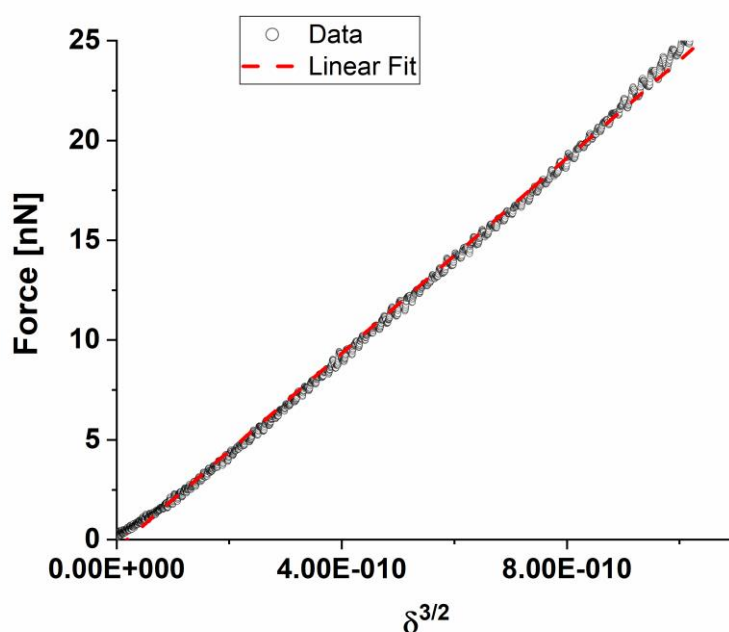


Figure 4-8. F - $d^{3/2}$ curve for a measurement performed with 5 $\mu\text{m/s}$, 25 nN maximum load on a 0.5 % Agarose gel with a spherical particle of 5 μm radius. The red dashed line indicates the linear fitting.

In **Figure 4-9**, all the fittings for the 0.5 % Agarose gel at a maximum force of 25 nN and loading rates from 0.25 to 25 $\mu\text{m/s}$ are shown. Overall, the fittings appear to perform very well over the whole indentation range, indicating isotropic mechanical properties of the agarose gel. As already expected from the Force-distance curves, no significant changes in the slopes seem to be apparent. All other fittings performed for the Agarose gels are not shown here to reduce redundancies. In **Table 4-1** and **Table 4-2**, a statistical analysis of the fittings can be seen. The calculated slopes appear to be normally distributed. For all measurements performed on 0.5% gels, no dependence of gel stiffness on loading rate was found.

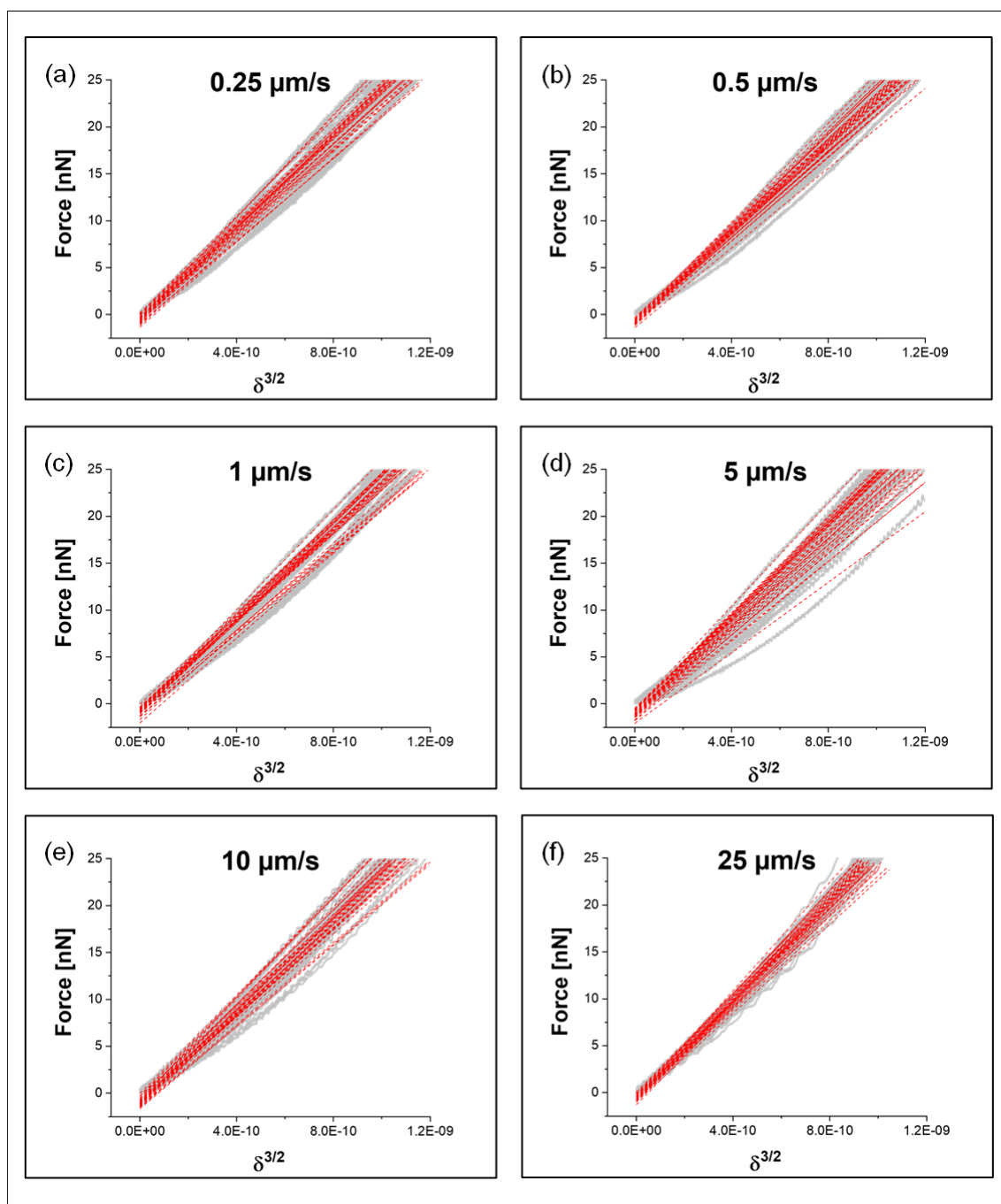


Figure 4-9 Fittings of 0.5 % agarose gel measured with a spherical particle of 5 μm radius at a maximum load of 25 nN and with loading rates ranges from 0.25 to 25 $\mu\text{m/s}$. Grey lines indicate the measurement data, while the red lines show the linear fittings.

Table 4-1. Overview of the fitted slopes. The maximum load was 25 nN and the gel's concentration 0.5%.

Velocity [$\mu\text{m/s}$]	N	Mean [$\text{N/m}^{3/2}$]	Standard Deviation	Minimum	Median	Maximum
0.25	32	24.04	0.22	21.96	24.05	27.19
0.5	34	23.78	0.19	21.22	23.84	26.33
1	33	24.06	0.20	21.82	24.10	26.60
2.5	34	23.86	0.22	21.30	23.71	27.39
5	35	24.12	0.25	20.88	24.46	27.46
10	34	24.42	0.24	21.61	24.41	27.50
25	34	25.98	0.19	23.65	25.99	28.90

Table 4-2. Statistical overview of the quality of the fittings. The maximum loading rate was 25 nN and the gel concentration 0.5%.

Velocity [$\mu\text{m/s}$]	N	Mean	Standard Deviation	Minimum	Median	Maximum
0.25	32	0.997	0.003	0.988	0.998	1.000
0.5	34	0.996	0.002	0.989	0.996	0.999
1	33	0.994	0.005	0.975	0.995	0.999
2.5	34	0.993	0.005	0.974	0.994	0.998
5	36	0.993	0.005	0.971	0.993	0.998
10	34	0.993	0.004	0.986	0.993	0.999
25	34	0.995	0.003	0.988	0.995	0.999

In a next step, the same analysis was performed for the 1.5% gel. As there were anisotropic mechanical properties visible in the curves (no linear shape), only the first 100 nm of the curves were used for fitting procedures. **Figure 4-10** shows the fittings for measurements

performed with a maximum load of 25 nN. Over the range of 100 nm, the fittings perform very well. **Table 4-3** and **Table 4-4** show the statistical analysis of the fittings.

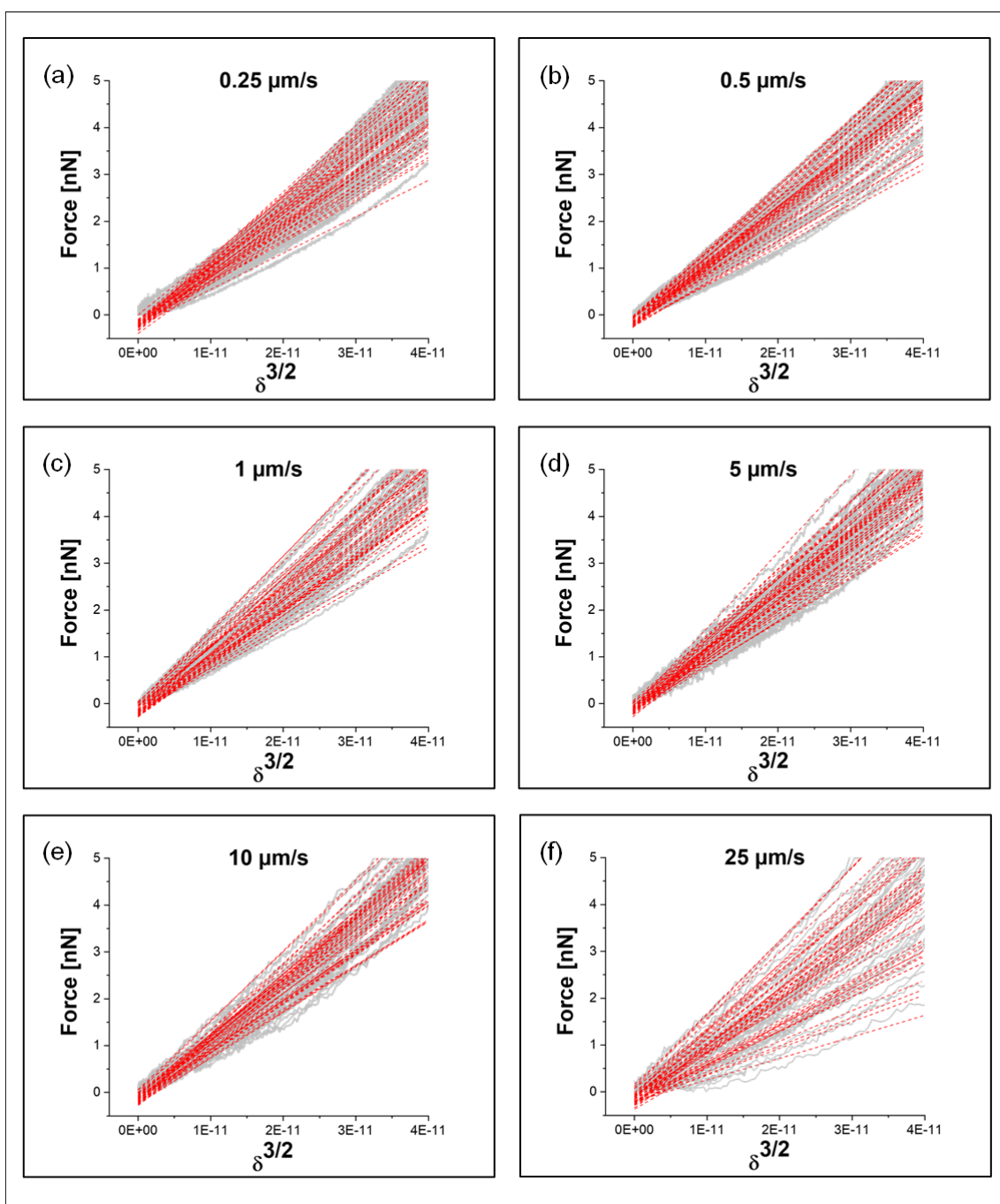


Figure 4-10 Fittings of 1.5 % agarose gel measured with a spherical particle at a maximum load of 25 nN and with loading rates ranges from 0.25 to 25 $\mu\text{m/s}$. Grey lines indicate the measurement data, while the red lines show the linear fits.

Table 4-3 Overview of the fitted slopes. The maximum load was 25 nN and the gel's concentration 1.5%.

Velocity [$\mu\text{m/s}$]	N	Mean [$\text{N/m}^{3/2}$]	Standard Deviation	Minimum	Median	Maximum
0.25	43	113.57	14.90	77.62	114.90	141.71
0.5	46	117.54	15.68	82.75	118.80	143.16
1	43	122.67	16.27	87.80	121.12	160.58
2.5	36	99.65	17.87	63.24	102.33	135.74
5	46	122.48	15.17	93.15	123.71	164.96
10	46	120.62	14.21	93.43	123.25	151.10
25	47	107.16	27.09	45.92	108.94	163.41

Table 4-4 Statistical overview of the quality of the fittings. The maximum loading rate was 25 nN and the gel concentration 0.5%.

Velocity [$\mu\text{m/s}$]	N	Mean	Standard Deviation	Minimum	Median	Maximum
0.25	43	0.988	0.007	0.969	0.990	0.998
0.5	46	0.990	0.007	0.973	0.992	0.999
1	43	0.990	0.006	0.976	0.992	0.999
2.5	36	0.983	0.010	0.953	0.985	0.999
5	46	0.990	0.005	0.977	0.990	0.997
10	46	0.988	0.008	0.957	0.990	0.998
25	47	0.980	0.018	0.901	0.985	0.999

As for the 0.5% gel, the fittings perform very well and the calculated slopes are approximately 5 to 6 times larger than the ones for the softer gel. The data is normally distributed, but the data for the stiff gel shows larger spreading than the soft one.

4.1.1.4. YOUNGS MODULUS

For the agarose gels the geometrical constant, derived by the radius of the sphere (5 μm), and the Poisson number ($\nu= 0.5$), was 251.6. This number is multiplied with the slope to obtain the Young's Modulus. **Table 4-5** and **Table 4-6** show the calculated Young's Moduli for the 0.5 and the 1.5% gel.

Table 4-5. Young's Modulus (in Pa) for the 0.5 % Agarose gel.

Velocity [$\mu\text{m/s}$]	N	Mean [Pa]	Standard Error
0.25	32	6048.94	55.25
0.5	34	5981.84	48.16
1	33	6054.63	49.49
2.5	34	6003.78	54.44
5	36	6031.62	71.81
10	34	6123.88	60.85
25	34	6537.21	48.07

Table 4-6. Young's Modulus (in Pa) for the 1.5 % Agarose gel.

Velocity [$\mu\text{m/s}$]	N	Mean [Pa]	Standard Error
0.25	43	28573.00	571.62
0.5	46	29573.77	581.68
1	43	30862.99	624.44
2.5	36	25072.19	749.39
5	46	30816.29	562.75
10	46	30347.96	527.18
25	47	26962.10	994.18

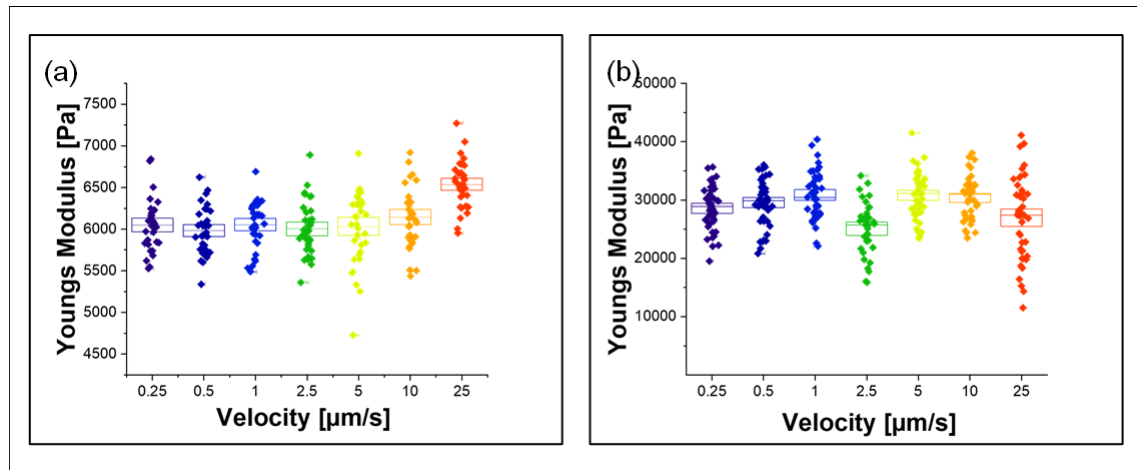


Figure 4-11 Young's Modulus of agarose gels at (a) 0.5% and (b) 1.5%. The graphs show a scatter plot with the standard error times 1.5 displayed as box. The line in between the standard error box is the median. The measurements raise from 0.25 to 25 $\mu\text{m/s}$ with a maximum loading rate of 25 nN.

Figure 4-11 shows the Young's Modulus calculated for both gels for the studied loading rates. The Modulus is approximately 6 kPa for the low concentration gel and 30 kPa for the higher concentrated one. Interestingly, for the 0.5 % gel, first a plateau for rates of 0.25 to 5 $\mu\text{m/s}$ can be seen, followed by a slight increase for 10 and 25 $\mu\text{m/s}$, with the final value being as high as 6.5 kPa. This could indicate that the gel behaves in a frequency dependent manner. For the 1.5 % gel, the values appear similar for all studied loading rates. The data at 2.5 $\mu\text{m/s}$ appears to be an outlier, as it is much lower than the other data points.

The here determined values for the gel stiffness at the defined concentrations are similar to what was already shown in literature, using AFM or a plate rheometer [63]. In literature, no evidence was found for the appearance of an increase of Young's Modulus with loading rate that would hint towards a viscoelastic behaviour.

4.2. BACTERIAL MECHANICS

The *E. coli* bacteria cells were measured with a cantilever that had a small, pyramidal tip at its end. Due to the small indentation of only a few ten nanometers and the tip having a comparable curvature, the contact geometry was assumed to be parabolic. All evaluation steps were performed in Origin and in R. Measurements were performed with loading rates ranging from 0.5 to 32 $\mu\text{m/s}$ and a maximum load of 1 nN. For Young's Modulus evaluation, an indentation of 20 nm was used.

4.2.1. FORCE-DISTANCE CURVES

Figure 4-12 shows representative force-distance curves for the different loading rates and all curves in the same plot for the measurements done on bacteria. The colour coding changes from purple to red with increased loading rate. Apparently, there is a slope increase with loading rate. As the indentations are only a few dozen nm, curves appear quite noisy. As the curves are that noisy, no curve averaging was performed.

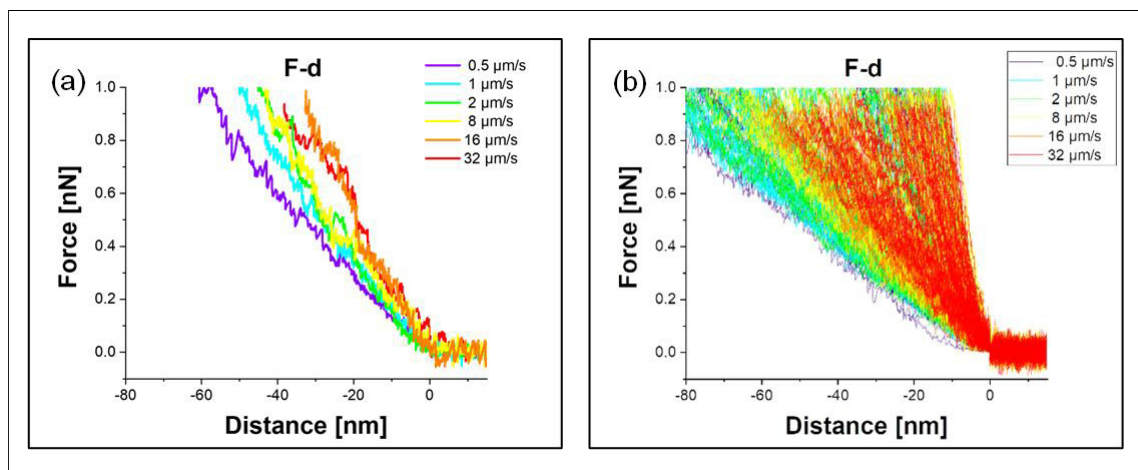


Figure 4-12 (a) Representative force-distance curves for each velocity. (b) All measured force-distance of all measured velocities combined in one graph. The approach speeds of 10 and 32 $\mu\text{m/s}$ show the steepest slopes, which indicates higher stiffness.

Figure 4-13 shows all the measurements separated for different tip velocities. The higher the velocity the steeper the slope of the curves. For the different loading rates, large spreads of data are visible.

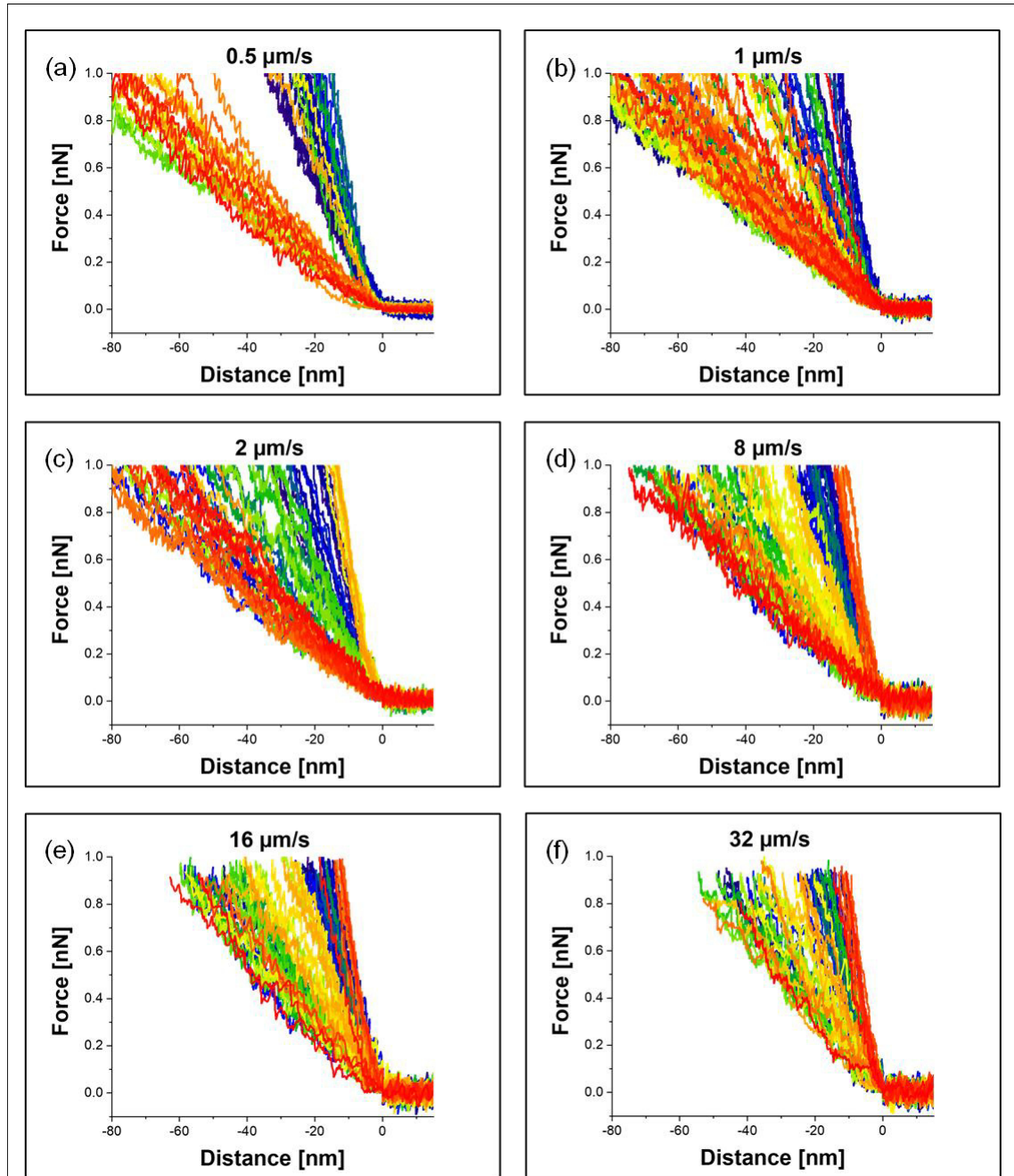


Figure 4-13 Force-distance-curves of bacteria measured with a tip of 10 nm radius at a maximum load of 1 nN and with loading rates ranging from 0.5 to 32 $\mu\text{m/s}$. Each colour represents a single measurement.

4.2.2. FITTINGS OF THE FORCE-DISTANCE^{3/2} CURVES FOR BACTERIA

Linear fittings were performed with the F vs $\delta^{3/2}$ curves over an indentation range of 20 nm.

Figure 4-14 shows these curves together with all the fittings.

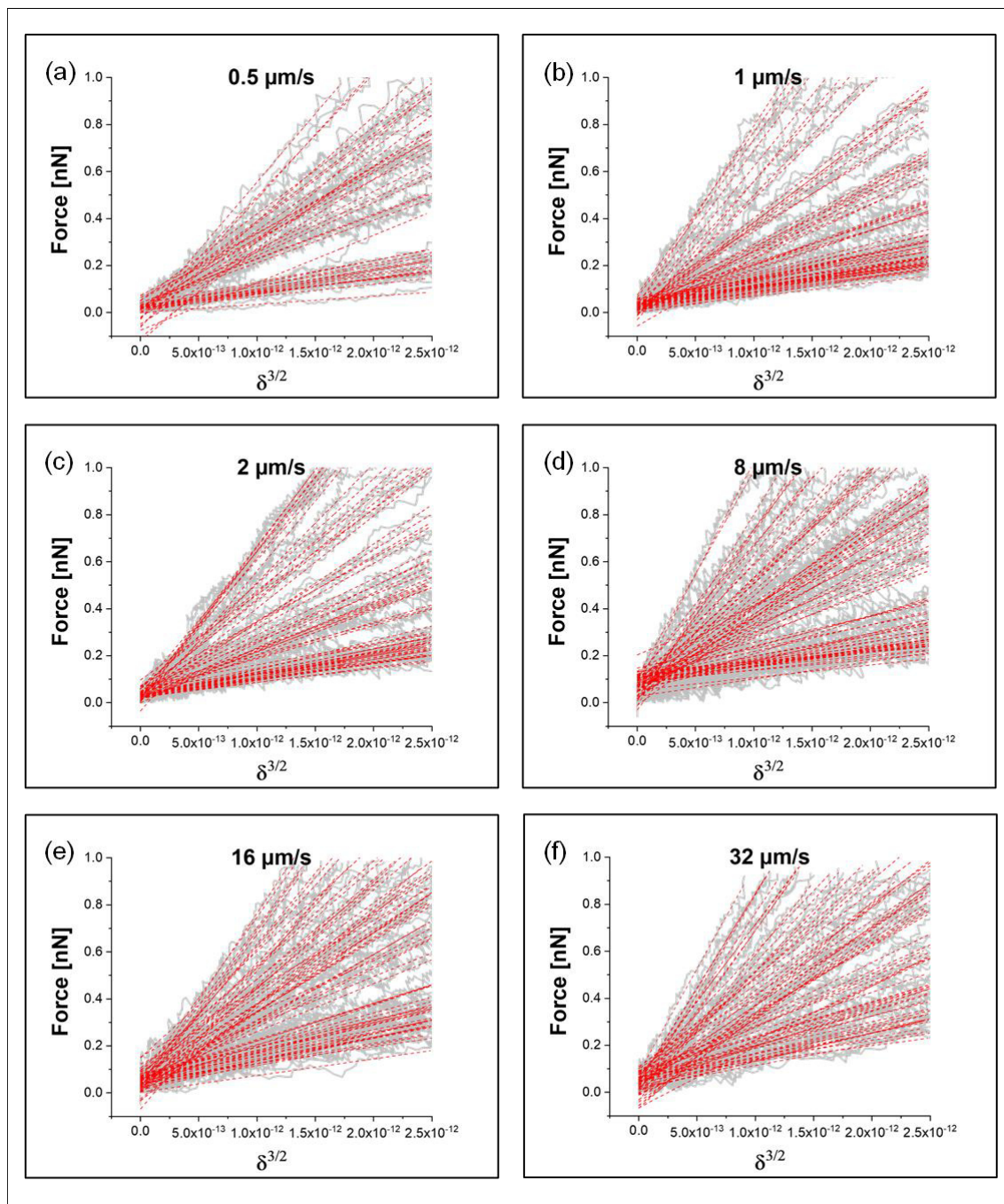


Figure 4-14. F - $d^{3/2}$ -curves and linear fittings of *E. coli* cells at a maximum load of 1 nN and with loading rates ranging from 0.5 to 32 $\mu\text{m/s}$. Grey lines indicate the measurement data, while the red lines show the linear fits over a range of 20 nm.

Table 4-7 and **Table 4-8** show the results of the fittings. They appear to perform quite well with an R2 of around 0.95, considering the small indentations and therefore high relative noise level. The values nevertheless show quite high variance and appear to be not normally distributed. Apparently, a lognormal distribution is better able to describe this distribution. An increase of the mean slope with the indentation range can be seen.

Table 4-7 Overview of the fitted slopes for bacterial measurements. The maximum load was 1 nN.

Velocity [$\mu\text{m/s}$]	N	Mean [$\text{N/m}^{3/2}$]	Standard Deviation	Minimum	Median	Maximum
0.5	41	221.81	153.36	34.63	201.96	581.21
1	70	208.78	183.65	57.91	111.60	764.65
2	63	235.69	185.66	52.07	182.12	658.82
8	72	271.67	226.96	43.71	207.89	957.07
16	70	293.73	184.87	71.02	287.14	744.54
32	68	322.52	214.98	65.80	288.43	888.48

Table 4-8 Statistics overview of the quality of the fittings over 20 nm indentation range for bacteria measurements.

Velocity [$\mu\text{m/s}$]	N	Mean	Standard Deviation	Minimum	Median	Maximum
0.5	41	0.967	0.029	0.871	0.974	0.993
1	70	0.954	0.036	0.850	0.962	0.994
2	63	0.950	0.055	0.636	0.965	0.996
8	72	0.978	0.015	0.895	0.981	0.993
16	70	0.953	0.042	0.833	0.975	0.994
32	68	0.952	0.043	0.786	0.968	0.995

4.2.3. YOUNGS MODULUS OF E. COLI

For a parabolic indenter with a radius of 10 nm, the value that the slope must be multiplied with is 5,625. Therefore, the calculated Modulus values are in the range of MPa. **Table 4-9** shows the Young's Moduli for the bacteria. **Figure 4-15** shows the calculated Young's Modulus values for the bacterial cells. An increase with loading rate can be seen.

Table 4-9. Young's Modulus (in Pa) for the bacterial measurements.

Velocity [$\mu\text{m/s}$]	N	Mean [Pa]	Standard Error
0.5	41	8.82E5	9.53E4
1	70	8.30E5	8.73E4
2	63	9.37E5	9.30E4
8	72	1.08E6	1.06E5
16	70	1.17E6	8.79E4
32	68	1.28E6	1.04E5

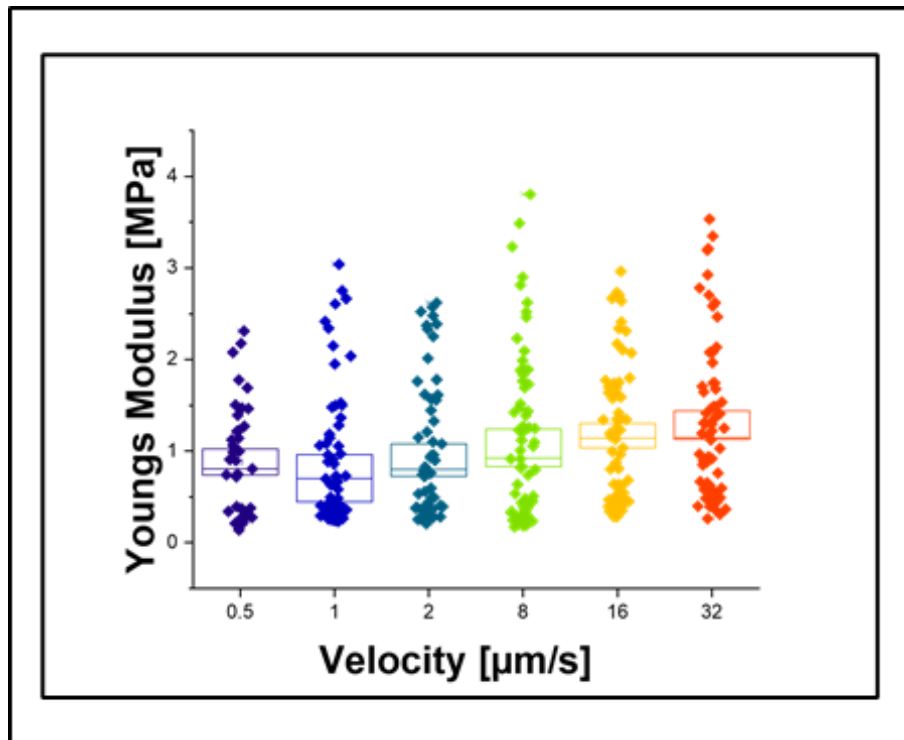


Figure 4-15. Calculated Young's Modulus for 20 nm indentation using a parabolic contact profile with an indenter radius of 10 nm. The boxes range from the 1st to the 3rd quartile.

The Young's Modulus lies between 0.8 (1 μm/s) and 1.2 MPa (32 μm/s). It increases with the approach speed. There is evidently a dependence on the loading rate and therefore a viscous fraction, which needs to be considered when determining the mechanical properties of bacteria.

The values shown here agree well with values published in literature. Also the power law behaviour that is shown here, meaning the increase of Young's Modulus with loading rate, is supported by an article [50]. Using only a parabolic shape for data analysis probably underestimates the Young's Modulus at the given indentation depth. A more accurate, but largely more complex, evaluation strategy would be to use the model of a blunted pyramidal tip [64]. As the error that is introduced by the parabolic simplification is always the same at the same indentation depth, this was omitted here.

4.3. MCF-7 CELL MECHANICS

For measurement of the mechanical properties of MCF-7 epithelial breast cancer cells, a silica particle with a radius of $5\ \mu\text{m}$ was used. Measurements were done with loading rates ranging from 1 to $32\ \mu\text{m/s}$ and a maximum load of 1 nN.

4.3.1. FORCE DISTANCE CURVES

Figure 4-16 shows all the force distance curves measured at the different loading rates.

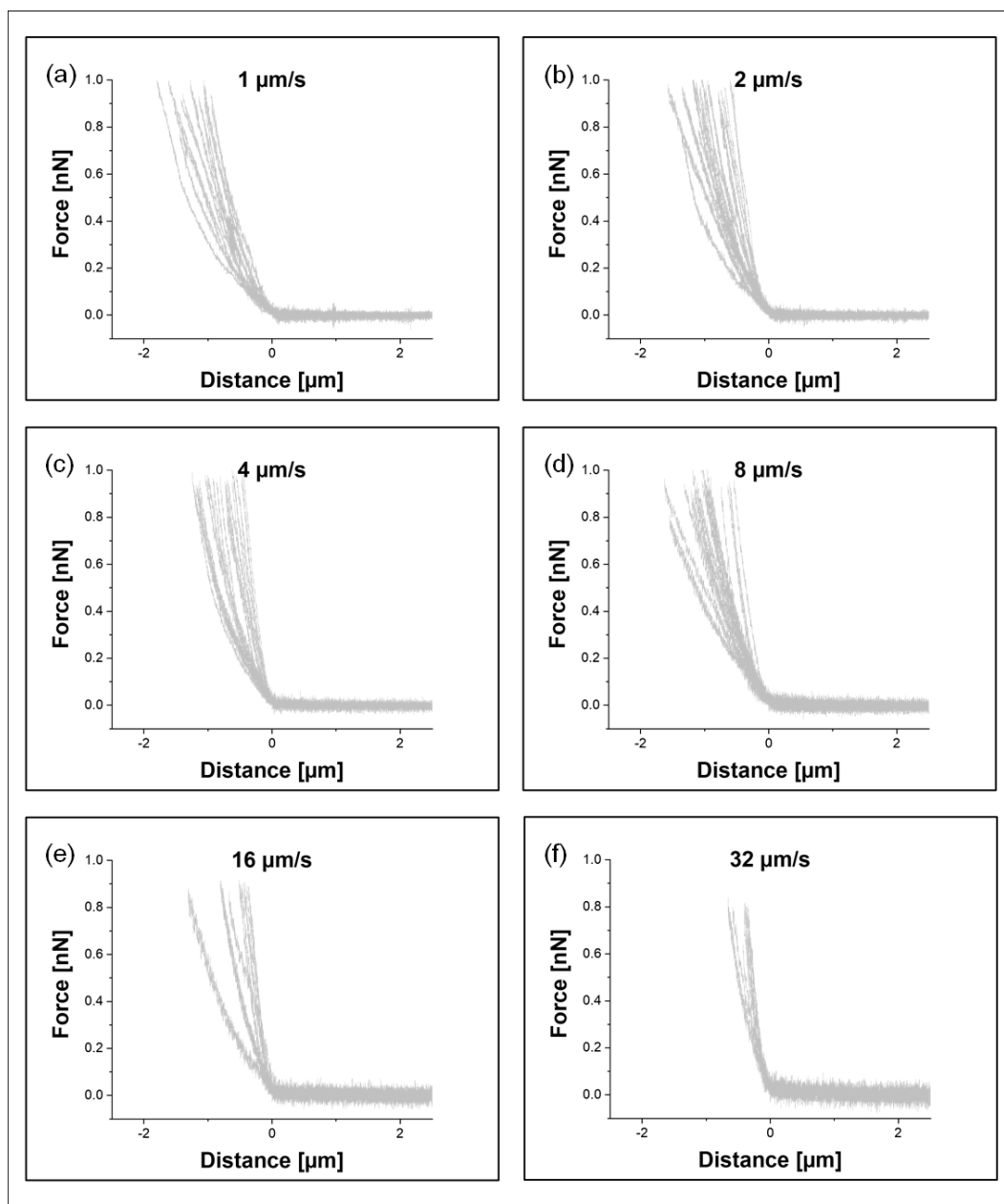


Figure 4-16. Force-distance curves measured on MCF-7 breast cancer cells with loading rates from 1 to $32\ \mu\text{m/s}$. Note that all the curves are scaled similar.

There is a decrease in the resulting cell indentation at the same force, hinting towards cells showing viscoelastic properties and behaving stiffer when they are pressed at higher frequencies. **Figure 4-17** shows the averages of the curves at the different loading rates, indicating an increase in slope.

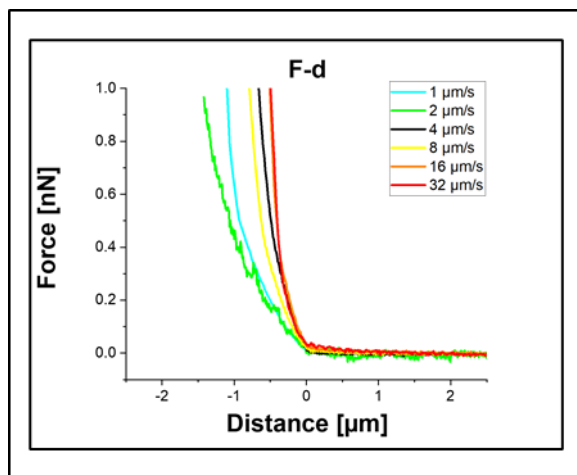


Figure 4-17. Averaged Force-distance curves for the different loading rates measured on cells with a maximum load of 1 nN.

4.3.2. FITTINGS OF THE FORCE-DISTANCE^{3/2} CURVES FOR MCF-7

In a next step, the mechanical elastic properties of the MCF-7 cells were determined using Origin by performing linear fits to the $F vs \delta^{3/2}$ curves. Cells are known to be anisotropic materials that have a complex, multi-layered structure. Therefore, the cell mechanical properties were evaluated using different indentation ranges of 250 and 500 nm. The MCF-7 cells are approximately 6 μm high, therefore these indentations are below the limit of 10% cell height normally used in literature for diminishing substrate artefacts. The values shown for these indentations are overestimation of approximately 15% due to substrate artefacts.

Figure 4-18 shows the fittings performed for the curves over 250 nm. **Table 4-10** and **Table 4-11** show the statistics of the fitting. Overall, the fitting performs well with goodness of fit values around 0.90. An increase in slope can be seen. Only the values for 8 $\mu\text{m/s}$ appear to be outliers, as they are lower than the other values.

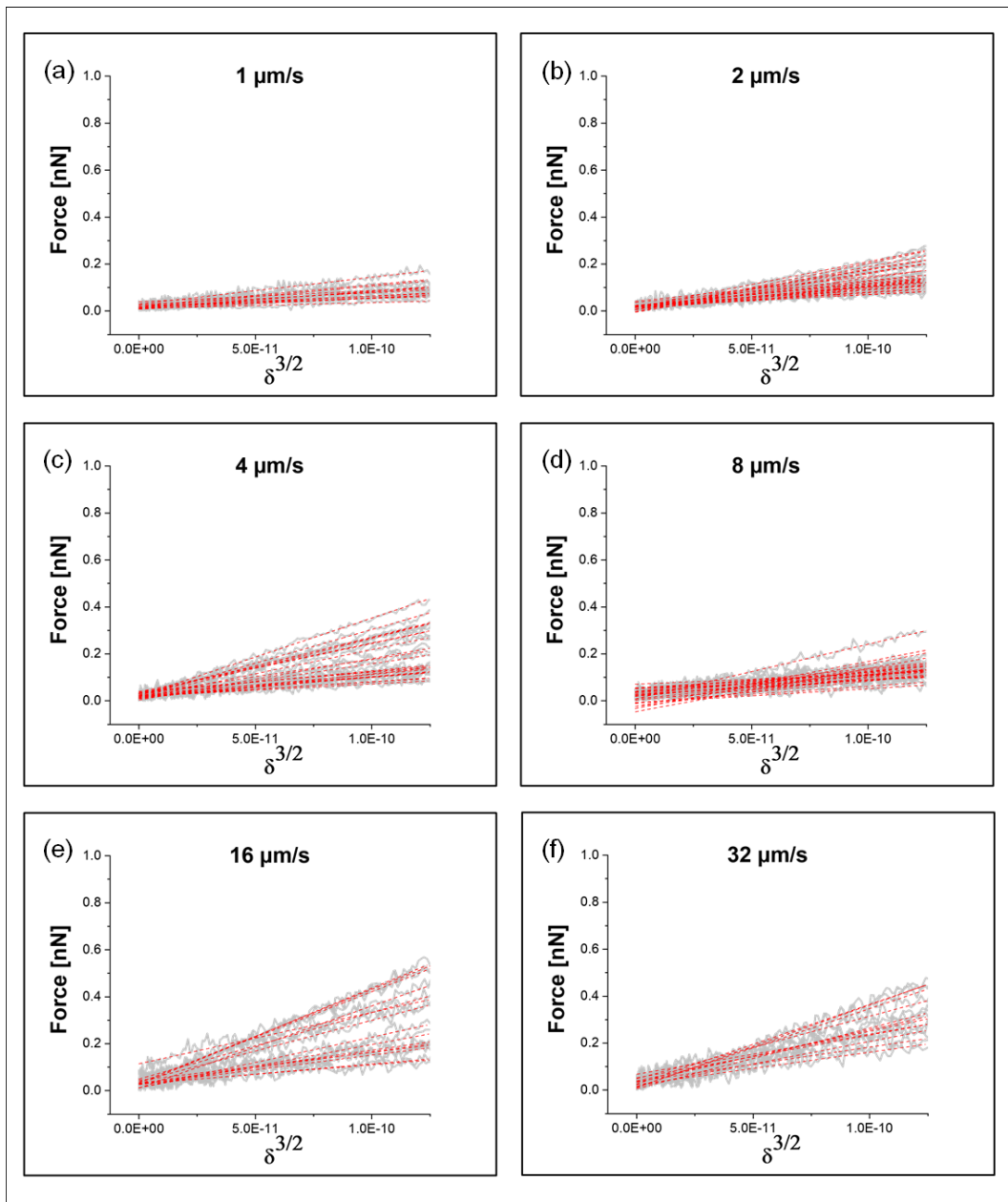


Figure 4-18. F - $d^{3/2}$ -curves and linear fittings to determine the elastic Modulus for measurements using a spherical particle and loading rates from 1 to 32 $\mu\text{m/s}$ for cells. The units for the x-axis are $\text{m}^{3/2}$.

Table 4-10. Overview of the fitted slopes for 250 nm of indentation of cells.

Velocity [$\mu\text{m/s}$]	N	Mean [$\text{N/m}^{3/2}$]	Standard Deviation	Minimum	Median	Maximum
1	14	0.64	0.20	0.30	0.64	0.98
2	26	1.09	0.46	0.50	0.93	2.07
4	23	1.48	0.83	0.53	1.05	3.32
8	27	0.96	0.49	0.37	0.88	2.33
16	15	2.27	1.16	0.81	2.16	4.11
32	12	2.34	0.75	1.38	2.18	3.52

Table 4-11. Overview of statistics of fitting cell mechanical properties over a range of 250 nm.

Velocity [$\mu\text{m/s}$]	N	Mean	Standard Deviation	Minimum	Median	Maximum
1	14	0.990	0.007	0.978	0.992	0.998
2	26	0.920	0.058	0.806	0.928	0.990
4	23	0.913	0.070	0.783	0.903	0.995
8	27	0.988	0.020	0.896	0.994	0.998
16	15	0.913	0.083	0.749	0.947	0.988
32	12	0.928	0.037	0.865	0.933	0.975

In a second step, linear fittings were performed over an indentation range of 500 nm. These can be seen in **Figure 4-19**. The statistics summary of the fittings is shown in **Table 4-12** and **Table 4-13**. The fittings perform slightly better with goodness of fitting values around 0.95. As before, the slope of the curves appears to increase with loading rate and the slopes are like the analysis performed with 250 nm. Like before, the values for 8 $\mu\text{m/s}$ appear to be outliers.

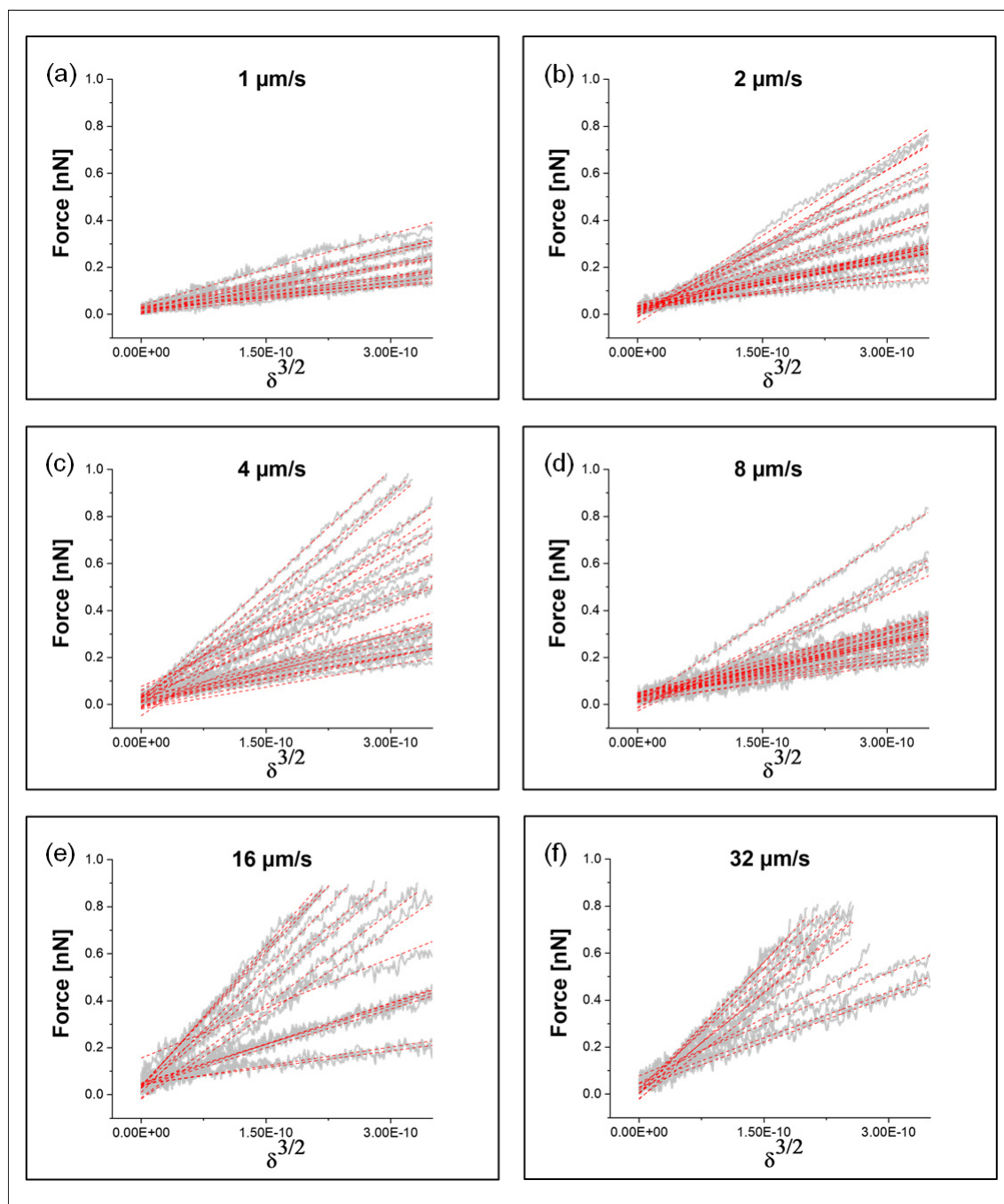


Figure 4-19. Linear fittings for $F\text{-}\delta^{3/2}$ -curves measured on cells with a fitting range of 500 nm.

Table 4-12. Summary of linear fittings performed over 500 nm for cell measurements.

Velocity [$\mu\text{m/s}$]	N	Mean [$\text{N/m}^{3/2}$]	Standard Deviation	Minimum	Median	Maximum
1	14	0.59	0.22	0.31	0.54	1.00
2	26	1.05	0.57	0.34	0.76	2.27
4	23	1.48	0.83	0.62	1.33	3.24
8	27	0.92	0.44	0.51	0.84	2.31
16	15	2.20	1.27	0.47	2.40	4.01
32	12	2.62	0.92	1.29	2.85	3.73

Table 4-13. Summary of statistics of the fittings performed over 500 nm for cell measurements.

Velocity [$\mu\text{m/s}$]	N	Mean	Standard Deviation	Minimum	Median	Maximum
1	14	0.967	0.016	0.940	0.970	0.989
2	26	0.975	0.024	0.871	0.979	0.997
4	23	0.987	0.010	0.968	0.988	0.999
8	27	0.963	0.020	0.924	0.966	0.997
16	15	0.969	0.042	0.860	0.989	0.996
32	12	0.980	0.006	0.972	0.979	0.990

4.3.3. YOUNG'S MODULUS OF MCF-7

Finally, the elastic Modulus was calculated for the MCF-7 cells. The result of this analysis can be seen in **Table 4-14** and **Table 4-15**, and **Figure 4-20** for both indentation ranges of 250 and 500 nm. There appears to be an increase in the value with loading rate.

Table 4-14. Young's Modulus (in Pa) for cell measurements at an indentation of 250 nm.

Velocity [$\mu\text{m/s}$]	N	Mean [Pa]	Standard Error
1	13	148.46	18.24
2	26	275.16	22.89
4	23	373.27	43.54
8	27	241.63	23.79
16	15	570.34	75.49
32	12	589.63	54.71

Table 4-15. Young's Modulus (in Pa) for the cell measurements at an indentation of 500 nm.

Velocity [$\mu\text{m/s}$]	N	Mean [Pa]	Standard Error
1	14	148.86	14.54
2	26	264.51	27.92
4	23	371.94	43.35
8	27	230.68	21.30
16	15	553.17	82.46
32	12	660.21	66.58

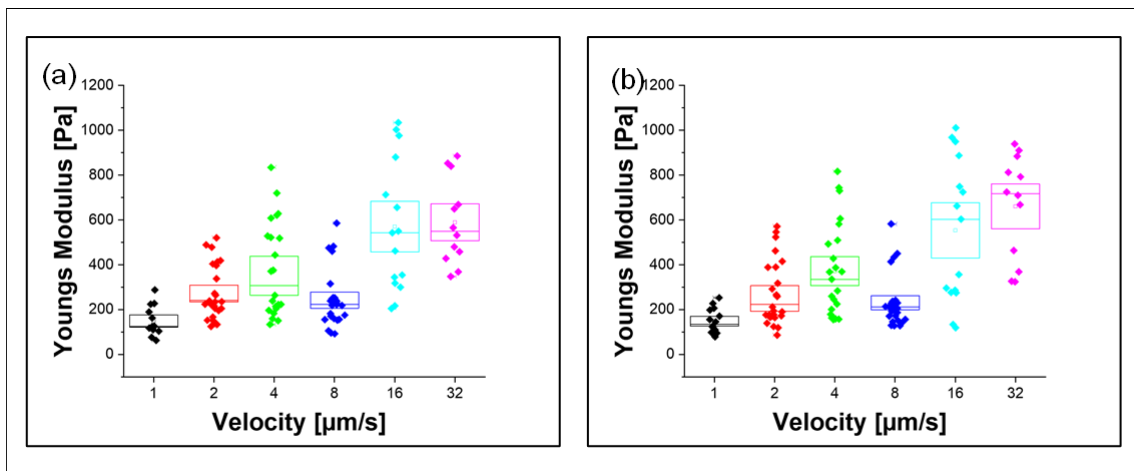


Figure 4-20 (a) Young's modulus of MCF-7 cells at an indentation of 250 nm. (b) Modulus at an indentation of 500 nm. Both were measured with a 10 μm spherical particle and an approach speed of 1 to 32 $\mu\text{m/s}$.

The calculated Young's Modulus for the cells are similar to what can be found in the literature, ranging from around 180 Pa for very slow measurements up to 700 Pa for the fastest measurements [24]. Again, a slight error was introduced in this simplified analysis, as there is an effect of the underlying stiff substrate that leads to an overestimation of approximately 18% at an indentation of 250 nm and 26% at 500 nm. As the same errors apply to the measurements at equal indentations, this error introduction was ignored here.

4.4. POWER LAW RHEOLOGY

Finally, I have evaluated the dependence of the measured Young's Modulus of all four different materials studied on the loading rate. For this, a Power Law Rheology model was used. **Figure 4-21** shows this analysis and **Table 4-16** shows the fitting parameters. Note that the axes are scaled logarithmically, and a power law behaviour is visible as a linear relationship.

Table 4-16. Power law rheology analysis.

Material	E_0 (Pa)	α	R^2	Adj. R^2
Cell	152.4	0.35	0.608	0.511
Bacteria	879,283.8	0.10	0.952	0.940
Gel 0.5 %	6,048.9	0.02	0.609	0.530
Gel 1.5 %	29,308.7	0.003	0.530	-0.193

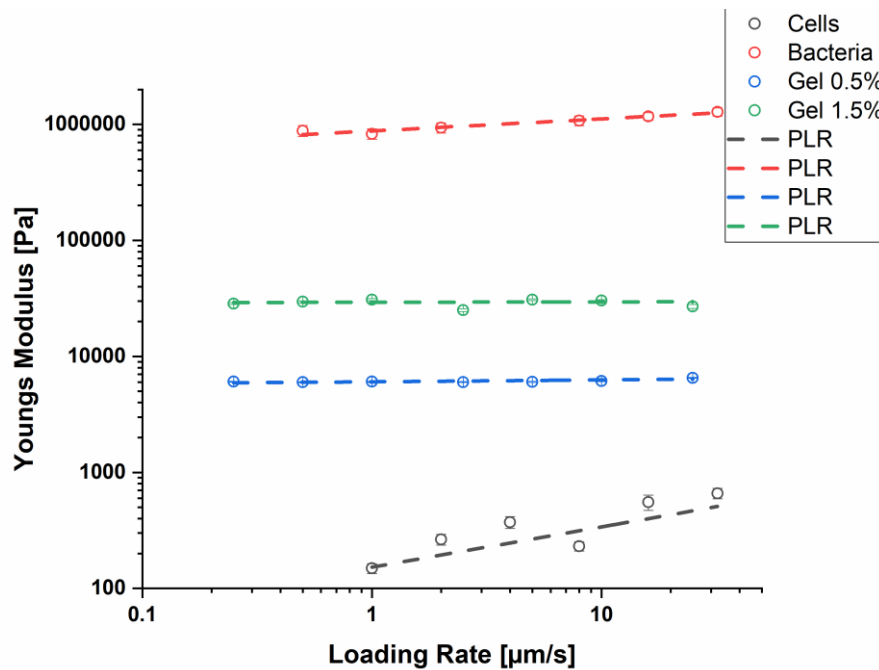


Figure 4-21. Power Law Rheology analysis of all studied materials. The dashed line indicates the power law fitting while the open circles indicate the Young's Modulus values and the error shown is the standard error.

From this analysis, multiple things can be considered. The gels appear to behave purely elastic in the studied range of frequency, as there is no dependence on the loading rate. This agrees well with the data the literature provides. In addition, the negative adjusted R^2 value shows that the proposed model is fitting the data for the stiffer gels worse than considering a constant function without slope. The Young's Modulus of the gels is constant at the studied frequency. For bacteria, a slight increase in the Young's Modulus can be seen that has a power law exponent of 0.10. This indicates that the bacteria behave as viscoelastic material with mostly elastic behaviour. Finally, for the cells a strong dependence on the loading can be seen with an exponent of 0.35. The low goodness of fit estimate for the cells stems from the fact that the data is quite spread.

5. CONCLUSIONS

In this work I have investigated the mechanical properties of Agarose gels, bacteria and epithelial breast cancer cells on the nano- and microscale using Atomic Force Microscopy. I have used elastic theory to determine the Young's Modulus of the material at different loading rates, ranging from around 0.2 to 30 $\mu\text{m/s}$. Cells appear to be the softest of these materials, with elastic Modulus values of around 200 to 700 Pa, with a strong dependence on the used loading rate. The 0.5 % Agarose gel shows a Young's Modulus of 6 kPa, while the 1.5 % gel shows one of 30 kPa. Finally, bacteria appear to be the stiffest materials with Young's Modulus values of around 1 MPa.

The studied materials show differences in the Young's Modulus over six orders of magnitude, but are still all biological materials made up from self-assembly processes. The reason for this is that these materials are all organized in different ways. Cell mechanical properties is mostly determined by the actin cytoskeleton, that is found (among other structures) in the actomyosin cortex below the cell membrane. Inside the cell the cytoplasm is a crowded fluid structure, with many different types of molecules. It is therefore not surprising that at the used frequencies for this thesis, cells behave as very soft viscoelastic materials with a strong viscous influence. The cytoskeletal structures of cells behave as semiflexible polymer networks and therefore show quite soft properties.

For the investigated gels, no significant dependence of the measured mechanics on the loading rate was found. Gels have been described in literature as poroelastic materials. The major determinants of gel mechanical properties are the order and type of crosslinking the monomers that make up the gel that is hydrated by water. The crosslinking determines the porosity of the hydrogels and therefore also how much water is stored inside the material. When hydrogels are compressed, the water inside the pores is pushed along the compression field (and if the measurement is done in liquid, it is pushed out of the material). If the compression is not fast and large enough, one will therefore only measure the mechanical properties of the porous elastic polymer material. Only at high frequencies, viscoelastic properties are expected. Therefore, for the gels, using elasticity at the given frequencies makes sense.

Finally, the bacteria showed Young's Modulus values as high as MPa. These values fit together well with data shown in literature. The studied bacteria are gram-negative, therefore their cell wall is made up out of two membranes that are interspaced with a thin, stiff peptidoglycan layer. This layer is covalently and non-covalently connected to the outer membrane. As there is a large difference in concentration of molecules considering the

inside and the outside of bacteria, this leads to a strong pressure difference across the bacterial cell envelope. The strong mechanical properties of bacteria are determined by the organization of the peptidoglycan and the outer membrane. The peptidoglycan is a structure that is made from self-assembly of very stiff sugar chains that are cross-linked by quite flexible peptides. This structure gives the bacteria their strong mechanical phenotype. Interestingly, I show here that bacteria do not behave fully like elastic solids, but rather show viscoelastic solid-like properties.

Finally, looking towards the future, one could imagine investigating the role of hysteresis in the different materials. Hysteresis was visible in the cell and bacteria curves but not in the gel ones. It would be interesting to consider the effects of different loading rates, maximum loads and indenter geometries on the hysteresis, as this property can also be used to estimate the amount of viscous (and plastic) response during deformation experiments. In addition, time-dependent experiments of the gels, cells and bacteria can be used to quantify the viscoelastic properties.

6. REFERENCES

- [1] J. Eyckmans, T. Boudou, X. Yu, and C. S. Chen, “A hitchhiker’s guide to mechanobiology,” *Dev. Cell*, vol. 21, no. 1, pp. 35–47, 2011.
- [2] K. A. Jansen, D. M. Donato, H. E. Balcioglu, T. Schmidt, E. H. J. Danen, and G. H. Koenderink, “A guide to mechanobiology: Where biology and physics meet,” *Biochim. Biophys. Acta - Mol. Cell Res.*, vol. 1853, no. 11, Part B, pp. 3043–3052, 2015.
- [3] R. Horwitz, “Cellular Biophysics,” *Biophys. J.*, vol. 110, no. 5, pp. 993–996, 2016.
- [4] G. Y. H. Lee and C. T. Lim, “Biomechanics approaches to studying human diseases,” *Trends Biotechnol.*, vol. 25, no. 3, pp. 111–118, 2007.
- [5] J. D. Humphrey, “Continuum biomechanics of soft biological tissues,” *Proc. R. Soc. Lond.*, vol. 459, pp. 3–46, 2002.
- [6] E. Moeendarbary and A. R. Harris, “Cell mechanics: principles, practices, and prospects,” *Wiley Interdiscip. Rev. Syst. Biol. Med.*, vol. 6, no. 5, pp. 371–388, 2014.
- [7] B. Alberts, A. Johnson, J. Lewis, D. Morgan, M. Raff, and K. Roberts, *Molecular Biology of the Cell, Sixth Edition*. Garland Science: New York and Abingdon, UK 2014, 2014.
- [8] J. B. Grotberg, “Respiratory Fluid Mechanics and Transport Processes,” *Annu. Rev. Biomed. Eng.*, vol. 3, no. 1, pp. 421–457, Aug. 2001.
- [9] G. S. Kassab, “Biomechanics of the cardiovascular system: the aorta as an illustrative example,” *J. R. Soc. Interface*, vol. 3, no. 11, pp. 719–740, Dec. 2006.
- [10] A. P. Voorhees and H.-C. Han, “Biomechanics of Cardiac Function,” *Compr. Physiol.*, vol. 5, no. 4, pp. 1623–1644, Sep. 2015.
- [11] M. Chiong *et al.*, “Cardiomyocyte death: mechanisms and translational implications,” *Cell Death Dis.*, vol. 2, no. 12, pp. e244–e244, 2011.
- [12] E. Laurini *et al.*, “Biomechanical defects and rescue of cardiomyocytes expressing pathologic nuclear lamins,” *Cardiovasc. Res.*, vol. 114, no. 6, pp. 846–857, May 2018.
- [13] L. Valon, A. Marín-Llauradó, T. Wyatt, G. Charras, and X. Trepat, “Optogenetic control of cellular forces and mechanotransduction,” *Nat. Commun.*, vol. 8, 2017.
- [14] A. E. Ekpenyong *et al.*, “Viscoelastic Properties of Differentiating Blood Cells Are Fate- and Function-Dependent,” *PLoS One*, vol. 7, no. 9, p. e45237, Sep. 2012.
- [15] N. I. Petridou, Z. Spiró, and C.-P. Heisenberg, “Multiscale force sensing in development,” *Nat. Cell Biol.*, vol. 19, no. 6, pp. 581–588, 2017.
- [16] J. Fouchard *et al.*, “Curling of epithelial monolayers reveals coupling between active bending and tissue tension,” *Proc. Natl. Acad. Sci. U. S. A.*, vol. 117, no. 17, pp. 9377–9383, Apr. 2020.
- [17] G. Nardone *et al.*, “YAP regulates cell mechanics by controlling focal adhesion assembly,” *Nat. Commun.*, vol. 8, no. 1, p. 15321, 2017.
- [18] B. Fabry, G. N. Maksym, J. P. Butler, M. Glogauer, D. Navajas, and J. J. Fredberg, “Scaling the microrheology of living cells,” *Phys. Rev. Lett.*, vol. 87, no. 14, p.

148102, Oct. 2001.

- [19] Y. M. Efremov, T. Okajima, and A. Raman, "Measuring viscoelasticity of soft biological samples using atomic force microscopy," *Soft Matter*, vol. 16, no. 1, pp. 64–81, 2019.
- [20] P. Bursac *et al.*, "Cytoskeletal remodelling and slow dynamics in the living cell," *Nat. Mater.*, vol. 4, no. 7, pp. 557–561, 2005.
- [21] A. Weber, B. Zbiral, J. Iturri, R. Benitez, and J. L. Toca-Herrera, "Measuring (biological) materials mechanics with atomic force microscopy. 2. Influence of the loading rate and applied force (colloidal particles)," *Microsc. Res. Tech.*, vol. 84, no. 5, pp. 1078–1088, May 2021.
- [22] M. Sumarokova *et al.*, "Influencing the adhesion properties and wettability of mucin protein films by variation of the environmental pH," *Sci. Rep.*, vol. 8, no. 1, p. 9660, 2018.
- [23] A. Weber, J. Iturri, R. Benitez, and J. L. Toca-Herrera, "Measuring biomaterials mechanics with atomic force microscopy. 1. Influence of the loading rate and applied force (pyramidal tips)," *Microsc. Res. Tech.*, vol. 82, pp. 1392–1400, May 2019.
- [24] B. Zbiral, A. Weber, J. Iturri, M. d. M. Vivanco, and J. L. Toca-Herrera, "Estrogen Modulates Epithelial Breast Cancer Cell Mechanics and Cell-to-Cell Contacts," *Materials*, vol. 14, no. 11, 2021.
- [25] B. R. Brückner, H. Nöding, and A. Janshoff, "Viscoelastic Properties of Confluent MDCK II Cells Obtained from Force Cycle Experiments," *Biophys. J.*, vol. 112, no. 4, pp. 724–735, 2017.
- [26] D. E. Ingber, N. Wang, and D. Stamenović, "Tensegrity, cellular biophysics, and the mechanics of living systems," *Reports Prog. Phys.*, vol. 77, no. 4, p. 046603, 2014.
- [27] M. Arnoldi, M. Fritz, E. Bäuerlein, M. Radmacher, E. Sackmann, and A. Boulbitch, "Bacterial turgor pressure can be measured by atomic force microscopy.," *Phys. Rev. E, Stat. physics, plasmas, fluids, Relat. Interdiscip. Top.*, vol. 62, no. 1 Pt B, pp. 1034–1044, Jul. 2000.
- [28] N. Desprat, A. Richert, J. Simeon, and A. Asnacios, "Creep Function of a Single Living Cell," *Biophys. J.*, vol. 88, no. 3, pp. 2224–2233, 2005.
- [29] B. D. Hoffman and J. C. Crocker, "Cell mechanics: dissecting the physical responses of cells to force.," *Annu. Rev. Biomed. Eng.*, vol. 11, pp. 259–288, 2009.
- [30] C. T. Lim, E. H. Zhou, and S. T. Quek, "Mechanical models for living cells - A review," *J. Biomech.*, vol. 39, no. 2, pp. 195–216, 2006.
- [31] Y. M. Efremov, W.-H. Wang, S. D. Hardy, R. L. Geahlen, and A. Raman, "Measuring nanoscale viscoelastic parameters of cells directly from AFM force-displacement curves," *Sci. Rep.*, vol. 7, no. 1, p. 1541, 2017.
- [32] Y. M. Efremov *et al.*, "Anisotropy vs isotropy in living cell indentation with AFM," *Sci. Rep.*, vol. 9, no. 1, p. 5757, 2019.
- [33] S. Mondal, S. Das, and A. K. Nandi, "A review on recent advances in polymer and peptide hydrogels," *Soft Matter*, vol. 16, no. 6, pp. 1404–1454, 2020.
- [34] M. Mahinroosta, Z. Jomeh Farsangi, A. Allahverdi, and Z. Shakoori, "Hydrogels as

- intelligent materials: A brief review of synthesis, properties and applications,” *Mater. Today Chem.*, vol. 8, pp. 42–55, 2018.
- [35] E. M. Ahmed, “Hydrogel: Preparation, characterization, and applications: A review,” *J. Adv. Res.*, vol. 6, no. 2, pp. 105–121, 2015.
- [36] W. E. Hennink and C. F. van Nostrum, “Novel crosslinking methods to design hydrogels,” *Adv. Drug Deliv. Rev.*, vol. 64, pp. 223–236, 2012.
- [37] T. Billiet, M. Vandenhaute, J. Schelfhout, S. Van Vlierberghe, and P. Dubruel, “A review of trends and limitations in hydrogel-rapid prototyping for tissue engineering,” *Biomaterials*, vol. 33, no. 26, pp. 6020–6041, 2012.
- [38] C. D. Spicer, “Hydrogel scaffolds for tissue engineering: the importance of polymer choice,” *Polym. Chem.*, vol. 11, no. 2, pp. 184–219, 2020.
- [39] I. M. El-Sherbiny and M. H. Yacoub, “Hydrogel scaffolds for tissue engineering: Progress and challenges,” *Glob. Cardiol. Sci. Pract.*, vol. 2013, no. 3, pp. 316–342, Nov. 2013.
- [40] M. L. Oyen, “Mechanical characterisation of hydrogel materials,” *Int. Mater. Rev.*, vol. 59, no. 1, pp. 44–59, Jan. 2014.
- [41] A. M. Kloxin, C. J. Kloxin, C. N. Bowman, and K. S. Anseth, “Mechanical properties of cellularly responsive hydrogels and their experimental determination,” *Adv. Mater.*, vol. 22, no. 31, pp. 3484–3494, Aug. 2010.
- [42] A. J. Engler, S. Sen, H. L. Sweeney, and D. E. Discher, “Matrix elasticity directs stem cell lineage specification,” *Cell*, vol. 126, no. 4, pp. 677–689, Aug. 2006.
- [43] D. E. Discher, P. Janmey, and Y.-L. Wang, “Tissue cells feel and respond to the stiffness of their substrate,” *Science*, vol. 310, no. 5751, pp. 1139–43, 2005.
- [44] E. Moeendarbary *et al.*, “The cytoplasm of living cells behaves as a poroelastic material,” *Nat. Mater.*, vol. 12, no. 3, pp. 253–261, 2013.
- [45] Y. Hu and Z. Suo, “Viscoelasticity and poroelasticity in elastomeric gels,” *Acta Mech. Solida Sin.*, vol. 25, no. 5, pp. 441–458, 2012.
- [46] K. D. Young, “Bacterial morphology: why have different shapes?,” *Curr. Opin. Microbiol.*, vol. 10, no. 6, pp. 596–600, Dec. 2007.
- [47] M. Mathelié-Guinlet, A. T. Asmar, J.-F. Collet, and Y. F. Dufrêne, “Lipoprotein Lpp regulates the mechanical properties of the E. coli cell envelope,” *Nat. Commun.*, vol. 11, no. 1, p. 1789, 2020.
- [48] E. R. Rojas *et al.*, “The outer membrane is an essential load-bearing element in Gram-negative bacteria,” *Nature*, vol. 559, no. 7715, pp. 617–621, 2018.
- [49] T. J. Silhavy, D. Kahne, and S. Walker, “The bacterial cell envelope,” *Cold Spring Harb. Perspect. Biol.*, vol. 2, no. 5, pp. a000414–a000414, May 2010.
- [50] V. Vadillo-Rodríguez and J. R. Dutcher, “Viscoelasticity of the bacterial cell envelope,” *Soft Matter*, vol. 7, no. 9, pp. 4101–4110, 2011.
- [51] D. A. Fletcher and R. D. Mullins, “Cell mechanics and the cytoskeleton,” *Nature*, vol. 463, no. 7280, pp. 485–492, Jan. 2010.
- [52] A. N. Ketene, P. C. Roberts, A. A. Shea, E. M. Schmelz, and M. Agah, “Actin

- filaments play a primary role for structural integrity and viscoelastic response in cells,” *Integr. Biol.*, vol. 4, no. 5, p. 540, 2012.
- [53] M. Pachenari, S. M. Seyedpour, M. Janmaleki, S. B. Shayan, S. Taranejoo, and H. Hosseinkhani, “Mechanical properties of cancer cytoskeleton depend on actin filaments to microtubules content: Investigating different grades of colon cancer cell lines,” *J. Biomech.*, vol. 47, no. 2, pp. 373–379, 2014.
- [54] L. Chin, Y. Xia, D. E. Discher, and P. A. Janmey, “Mechanotransduction in cancer,” *Curr. Opin. Chem. Eng.*, vol. 11, pp. 77–84, Feb. 2016.
- [55] J. M. Northcott, I. S. Dean, J. K. Mouw, and V. M. Weaver, “Feeling Stress: The Mechanics of Cancer Progression and Aggression,” *Frontiers in Cell and Developmental Biology*, vol. 6, p. 17, 2018.
- [56] P. Sollich, “Rheological constitutive equation for model of soft glassy materials,” *Phys. Rev. E*, vol. 58, no. 1, pp. 738–759, 1998.
- [57] J. Alcaraz *et al.*, “Microrheology of human lung epithelial cells measured by atomic force microscopy,” *Biophys. J.*, vol. 84, no. 3, pp. 2071–2079, 2003.
- [58] G. Binnig, C. Quate, and C. Gerber, “Atomic Force Microscope,” *Physical Review Letters*, vol. 56, no. 9, pp. 930–933, 1986.
- [59] H.-J. Butt, B. Cappella, and M. Kappl, “Force measurements with the atomic force microscope: Technique, interpretation and applications,” *Surf. Sci. Rep.*, vol. 59, no. 1, pp. 1–152, 2005.
- [60] H.-J. Butt and M. Jaschke, “Calculation of thermal noise in atomic force microscopy,” *Nanotechnology*, vol. 6, pp. 1–7, 1995.
- [61] R. Benítez, S. Moreno-flores, V. J. Bolós, and J. L. Toca-Herrera, “A new automatic contact point detection algorithm for AFM force curves,” *Microsc. Res. Tech.*, vol. 76, no. 8, pp. 870–876, 2013.
- [62] R. Benítez, V. J. Bolós, and J. L. Toca-Herrera, “afmToolkit: an R Package for Automated AFM Force-Distance Curves Analysis,” *R J.*, vol. 9, no. December, pp. 291–308, 2017.
- [63] C. D. Markert *et al.*, “Characterizing the micro-scale elastic modulus of hydrogels for use in regenerative medicine,” *J. Mech. Behav. Biomed. Mater.*, vol. 27, pp. 115–127, 2013.
- [64] F. Rico, P. Roca-Cusachs, N. Gavara, R. Farré, M. Rotger, and D. Navajas, “Probing mechanical properties of living cells by atomic force microscopy with blunted pyramidal cantilever tips,” *Phys. Rev. E*, vol. 72, no. 2, p. 21914, Aug. 2005.

7. LIST OF FIGURES

Figure 2-1. Architecture of the bacterial cell wall. Left part of the figure shows gram-positive and right part shows gram-negative cells. Figure taken from Vadillo et al, Soft Matter, 2011.....	8
Figure 2-2. Stress-strain diagram of steel. First the steel is deforming elastically (linear region), then plastic deformation takes place. The Yield strength resembles the elastic limit. Up to this point the bar behaves linear elastic. After reaching the yield strength, strain increases more in comparison to the inflicted stress. When the stress would be released, purely elastic materials change back to their original shape. Past the yield strength, plastic deformation starts. All strains past this point are irreversible. The yield strength usually starts with plastic deformations and sudden hardening. At C is the breaking point. It is the highest strain a material can withstand. Further strain leads to a constriction in diameter and a loss in stress. The last point is the breaking point. The material fails and breaks apart.	12
Figure 2-4. (Left) Representation of spring with a defined Young's Modulus. (Right) Representation of a dashpot with a defined viscosity.	15
Figure 2-5 Kelvin-Voigt and Maxwell elements.....	16
Figure 3-1. Micrograph of MCF-7 cells grown for 24 hours on glass slides in the culture medium. The image was done in phase contrast microscopy mode, with a 20x air objective.....	20
Figure 3-2. Scanning Electron Microscopy Images of Cantilevers used in this study. (Left) MSCT tip (taken from manufacturer website). (Right) NP-O cantilever after particle glueing.	22
Figure 3-3. Cantilevers after the particle glueing step. (Left) FORTG cantilever with 10 μm diameter particle. (Right) NP-O B cantilever with 10 μm diameter silica particle.....	23
Figure 3-4. MCF-7 cells grown on glass slides for 24 hours. The black triangular shadow indicates the cantilever.....	26
Figure 3-5. Phase contrast microscopy image of bacteria immobilized on PEI-coated glass slides. Top left corner shows the triangular end of the cantilever. The coloured insets show QI mode images of the bacteria.	27
Figure 3-6. Curve manipulation steps. (a) Raw Force-distance curve, in red the approach and in blue the retract part can be seen. (b) Baseline correction. (c) Contact point definition. (d) Correction of cantilever bending.	28
Figure 3-7. Pooled F-d-curves after the correction steps for measurements on a 0.5% Agarose gel with a 5 μm radius silica particle, a maximum load of 25 nN and approach velocity of 1 $\mu\text{m/s}$	29

Figure 4-1. Force-distance-curves of 0.5 % w/v agarose gel measured with a spherical particle at a maximum load of 5 nN and with loading rate ranges from 0.25 to 25 $\mu\text{m/s}$. Grey lines indicate the measurement data, while the red lines show the averaged measurements.32

Figure 4-2 Force-distance-curves of 0.5 % agarose gel measured with a spherical particle at a maximum load of 25 nN and with loading rate ranges from 0.25 to 25 $\mu\text{m/s}$. Grey lines indicate the measurement data, while the red lines show the averaged measurements.33

Figure 4-3 Force-distance-curves of 0.5 % agarose gel measured with a spherical particle at a maximum load of 50 nN and with loading rate ranges from 0.25 to 25 $\mu\text{m/s}$. Grey lines indicate the measurement data, while the red lines show the averaged measurements.34

Figure 4-4 Force-distance-curves of 1.5 % agarose gel measured with a spherical particle at a maximum load of 5 nN and with loading rates ranges from 0.25 to 25 $\mu\text{m/s}$. Grey lines indicate the measurement data, while the red lines show the averaged measurements.35

Figure 4-5 Force-distance-curves of 1.5 % agarose gel measured with a spherical particle at a maximum load of 25 nN and with loading rate ranges from 0.25 to 25 $\mu\text{m/s}$. Grey lines indicate the measurement data, while the red lines show the averaged measurements.36

Figure 4-6 Force-distance-curves of 1.5 % agarose gel measured with a spherical particle at a maximum load of 50 nN and with loading rates ranges from 0.25 to 25 $\mu\text{m/s}$. Grey lines indicate the measurement data, while the red lines show the averaged measurements.37

Figure 4-7 These curves show the averaged force-distance curves of the previous measurements. On the left side is the 0.5% and on the right side the 1.5% agarose gel. These curves were measured at 5, 25, and 50 nN and with loading rates ranging from 0.25 to 25 $\mu\text{m/s}$. The indentation differs by concentration of the gel. (a,c,e) from 0.5 μm to 1.5 μm and (b,d,f) 0.1 μm to 0.4 μm . Colour coding indicates the different loading rates. Note that the x-axis is scaled differently for the two different gels.39

Figure 4-8. $F-d^{3/2}$ curve for a measurement performed with 5 $\mu\text{m/s}$, 25 nN maximum load on a 0.5 % Agarose gel with a spherical particle of 5 μm radius. The red dashed line indicates the linear fitting.....40

Figure 4-9 Fittings of 0.5 % agarose gel measured with a spherical particle of 5 μm radius at a maximum load of 25 nN and with loading rates ranges from 0.25 to 25 $\mu\text{m/s}$. Grey lines indicate the measurement data, while the red lines show the linear fittings.41

Figure 4-10 Fittings of 1.5 % w/v agarose gel measured with a spherical particle at a maximum load of 25 nN and with loading rates ranges from 0.25 to 25 $\mu\text{m/s}$. Grey lines indicate the measurement data, while the red lines show the linear fits.....	43
Figure 4-11 Young's Modulus of agarose gels at (a) 0.5% and (b) 1.5%. The graphs show a scatter plot with the standard error times 1.5 displayed as box. The line in between the standard error box is the median. The measurements raise from 0.25 to 25 $\mu\text{m/s}$ with a maximum loading rate of 25 nN.	46
Figure 4-12 (a) Representative force-distance curves for each velocity. (b) All measured force-distance of all measured velocities combined in one graph. The approach speeds of 10 and 32 $\mu\text{m/s}$ show the steepest slopes, which indicates higher stiffness.	47
Figure 4-13 Force-distance-curves of bacteria measured with a tip of 10 nm radius at a maximum load of 1 nN and with loading rates ranging from 0.5 to 32 $\mu\text{m/s}$. Each colour represents a single measurement.	48
Figure 4-14. F-d ^{3/2} -curves and linear fittings of E. coli cells at a maximum load of 1 nN and with loading rates ranging from 0.5 to 32 $\mu\text{m/s}$. Grey lines indicate the measurement data, while the red lines show the linear fits over a range of 20 nm.	49
Figure 4-15. Calculated Young's Modulus for 20 nm indentation using a parabolic contact profile with an indenter radius of 10 nm. The boxes range from the 1st to the 3rd quartile.	52
Figure 4-16. Force-distance curves measured on MCF-7 breast cancer cells with loading rates from 1 to 32 $\mu\text{m/s}$. Note that all the curves are scaled similar.	53
Figure 4-17. Averaged Force-distance curves for the different loading rates measured on cells with a maximum load of 1 nN.	54
Figure 4-18. F-d ^{3/2} -curves and linear fittings to determine the elastic Modulus for measurements using a spherical particle and loading rates from 1 to 32 $\mu\text{m/s}$ for cells. The units for the x-axis are m ^{3/2}	55
Figure 4-19. Linear fittings for F-d ^{3/2} -curves measured on cells with a fitting range of 500 nm.....	57
Figure 4-20 (a) Young's modulus of MCF-7 cells at an indentation of 250 nm. (b) Modulus at an indentation of 500 nm. Both were measured with a 10 μm spherical particle and an approach speed of 1 to 32 $\mu\text{m/s}$	60
Figure 4-21. Power Law Rheology analysis of all studied materials. The dashed line indicates the power law fitting while the open circles indicate the Young's Modulus values and the error shown is the standard error.....	61

8. LIST OF TABLES

Table 3-1. Cantilevers used to study the three different biological materials (gels, cells and bacteria).....	21
Table 3-2 Experiment setup for the 0.5% Agarose gel AFM measurements	25
Table 3-3 Experiment setup for the 1.5% Agarose gel AFM measurements	25
Table 4-1. Overview of the fitted slopes. The maximum load was 25 nN and the gel's concentration 0.5%.	42
Table 4-2. Statistical overview of the quality of the fittings. The maximum loading rate was 25 nN and the gel concentration 0.5%.....	42
Table 4-3 Overview of the fitted slopes. The maximum load was 25 nN and the gel's concentration 1.5%.	44
Table 4-4 Statistical overview of the quality of the fittings. The maximum loading rate was 25 nN and the gel concentration 0.5%.....	44
Table 4-5. Young's Modulus (in Pa) for the 0.5 % Agarose gel.	45
Table 4-6. Young's Modulus (in Pa) for the 1.5 % Agarose gel.	45
Table 4-7 Overview of the fitted slopes for bacterial measurements. The maximum load was 1 nN.....	50
Table 4-8 Statistics overview of the quality of the fittings over 20 nm indentation range for bacteria measurements.....	50
Table 4-9. Young's Modulus (in Pa) for the bacterial measurements.	51
Table 4-10. Overview of the fitted slopes for 250 nm of indentation of cells.	56
Table 4-11. Overview of statistics of fitting cell mechanical properties over a range of 250 nm.....	56
Table 4-12. Summary of linear fittings performed over 500 nm for cell measurements. ...	58
Table 4-13. Summary of statistics of the fittings performed over 500 nm for cell measurements.	58
Table 4-14. Young's Modulus (in Pa) for cell measurements at an indentation of 250 nm.	59
Table 4-15. Young's Modulus (in Pa) for the cell measurements at an indentation of 500 nm.....	59
Table 4-16. Power law rheology analysis.....	60

9. ACKNOWLEDGEMENTS

First off, I express my deepest gratitude to my supervisor Jose Luis Tocca-Herrera. Even though I started working with you prior to the lecture Biophysics, these lectures opened my eyes concerning science and you inspired me and changed my way of thinking. Furthermore, I appreciate the patience you had with me and for the support, materials and laboratory. You never held back a good advice.

“Stairway To Heaven - Rodrigo Y Gabriela” “Also sprach Zarathustra – Richard Strauss”

Andi, you were the reason why I wrote this thesis. I remember the night when we were out, close to Heiligenstadt, and you explained your PhD topics to me. That sounded so interesting, that it “fixed” me on. During the time of working with you, we had our differences, but when hard came to hard, you always listened, and supported me. I want to thank you for all the long walks and talks home, where we had philosophic discussions on our work, on the world and on everything. You helped me out in any way possible, therefore I want to thank you not just for your time, your mentorship but most of all on our deep friendship.

“You are simply the best – Tina Turner” “Böhse Onkelz – Auf gute Freunde”

Then there are Ulli and Babsi. We three will always be the “Jenseits von Eden Masters und Schlagerstars”. Coffee breaks with you two were most intriguing. You gave me mental support, whenever necessary, but were also fixed on the topic of small things. When my biological knowledge was tested, you showed the patience and explained me interesting fun facts of cells, bacteria, proteins and life itself. The time with you is well appreciated and I hope our friendship will last on for a minimum of seven more decades.

“Three is a magic number – Bob Dorough” and obviously “Du schaffst das schon – Klubb3”

Dear Krismers, you are hell of an awesome family and I got most lucky to be part of us! Since I know that I cannot write all the things of appreciations for you in here (would be another thesis) I will leave it at that.

“Tirol Concerto – Philip Glass” “Mein Apfelbäumchen – Reinhard Mey”